Construction of an Ab Initio Kinetic Model for Industrial Ethane Pyrolysis

Wenjie Sunand Mark Saeys
Dept. of Chemical and Biomolecular Engineering, National University of Singapore, Singapore 117576, Singapore

DOI 10.1002/aic.12446
Published online November 8, 2010 in Wiley Online Library (wileyonlinelibrary.com).

The industrial steam cracking of ethane was simulated using an ab initio kinetic model. The reaction network consists of 20 species and 150 reversible elementary reactions. The thermodynamic and kinetic parameters were obtained from ab initio CBS-QB3 and W1U calculations and agree well with available experimental data. Predicted C_2H_6, C_2H_4, and H_2 yields are within 5% of experimental data for the three sets of conditions tested. Though CH_4 yields and outlet temperatures are particularly sensitive to the accuracy of the kinetic parameters, they are simulated with an accuracy of better than 10%. Larger deviations for the C_3H_6 and C_2H_2 yields are attributed to the limited size of the reaction network. The effect of total pressure on the rate coefficients was evaluated using Quantum Rice-Ramsberger-Kassel theory with the Modified Strong-Collision approximation, and was found to be relatively minor for the reaction conditions tested. This study hence demonstrates the feasibility of simulating complex radical reactions using a predictive kinetic model derived from state-of-the-art quantum chemical calculations. © 2010 American Institute of Chemical Engineers
AIChE J, 57: 2458–2471, 2011
Keywords: ab initio calculations; ethane steam cracking; modeling

Introduction

Steam cracking of hydrocarbons is the dominant process for the production of light olefins and an important process for the production of aromatics.[1] Accurate kinetic models are required for the design and optimization of the steam cracking process, and models for feedstock ranging from light hydrocarbons, such as ethane and propane,[2–9] to heavier mixtures, such as naphtha[5,10,11] can be found in the literature. The accuracy of a kinetic model depends on the completeness of the reaction network and on the accuracy of its kinetic and thermodynamic parameters.[12,13] Steam cracking proceeds via a high temperature radical mechanism and in particular for heavier feedstock the reaction network can involve several hundreds of reactions.[13–16]

Three types of kinetic models are commonly used to describe steam cracking: empirical models,[10] molecular reaction models,[3,5,17] and kinetic models based on elementary reactions.[4,6,7,12,14,15,18] In principle, kinetic models based on elementary reactions should be preferred since they can be used outside the domain where their parameters have been fitted. However, the large number of kinetic and thermodynamic parameters required in elementary kinetic models limits the feasibility of building such models by fitting to experimental data. To limit the number of fitted or estimated parameters, group additivity models and group contribution methods have been developed for thermodynamic and kinetic parameters, respectively.[19–26] Alternatively, kinetic parameters can be estimated using structure-reactivity relationships, such as the Brønsted-Evans-Polanyi relation between activation energies and reaction enthalpies.[12,13,27] However, determining the required group additivity parameters and structure-reactivity

Correspondence concerning this article should be addressed to M. Saeys at chesm@nus.edu.sg.

Table 1. Ethane Steam Cracking Reactor Geometry and Process Conditions

	I*	II†	III‡
Ethane feed flow rate (kg/s)	0.63	0.0011	3.9
Steam to ethane ratio (kg/kg)	0.4	0.4	0.35
Inlet temperature (K)	978	950	898
Inlet pressure (atm)	3.0	2.0	3.5
Reactor length (m)	95	21.75	101
Reactor diameter (int) (m)	0.108	0.01	0.124 (Pass 1–6) 0.136 (Pass 7–8)
Average heat flux (kW/m^2)§	63.1	5.6	75.4

*Reference 3.
†References 2 and 3.
‡Reference 39.
§Determined from a reactor energy balance.

relationships for complex kinetic models remains challenging and introduces additional uncertainties.

With the development of computational chemistry, it has become possible to rapidly calculate thermodynamic and kinetic parameters with reasonable accuracy. Indeed, accurate thermodynamic properties have been calculated with a variety of computational methods.[28–30] Using the CBS-QB3 method, the standard enthalpy of formation of hydrocarbons could be calculated with an accuracy of 2.5 kJ/mol.[31] Entropies and heat capacities of hydrocarbons can be predicted with an accuracy of a few J/mol K using an ab initio one-dimensional hindered rotor approach.[32] Kinetic parameters can also be predicted accurately. Hydrogen abstraction reaction rate coefficients have been calculated using transition state theory including quantum mechanical tunneling corrections and are typically within a factor four of experimental data over a wide range of temperatures.[24,33–35] Ab initio rate coefficients for carbon-centered radical addition reactions and for the reverse β-scission reactions also agree well with available experimental data.[36] The third important reaction family for steam cracking, radical–radical recombination reactions, has been studied using ab initio variable reaction coordinate transition state theory (VRC-TST), and rate coefficients for hydrogen-hydrocarbon radical recombination reactions[37] and for alkyl–alkyl radical recombination reactions[38] could be predicted accurately.

In this work, we illustrate that the accuracy that can be obtained with standard computational chemistry calculations has become sufficient to begin to predict the conversion and selectivity for a complex, high temperature gas phase radical process such as ethane steam cracking. Ethane steam cracking was selected because it is an example of a complex gas phase radical reaction for which pilot scale and industrial experimental data have been published (Table 1).[2,3,39] Moreover, compared to naphtha and vacuum gasoil cracking, the feed composition is well defined, and the size of the reaction network remains manageable. This then allows calculating all the individual kinetic and thermodynamic parameters in the model directly from first principles.

Modeling Methodology

Reaction network

The reaction network used in this work consists of 20 species and 150 reversible elementary reactions. Ten radicals (·H, $\cdot CH_3$, $\cdot C_2H_3$, $\cdot C_2H_5$, $\cdot C_3H_5$ (allyl), $\cdot C_3H_7$ (1-propyl), $\cdot 2\text{-}C_3H_7$ (2-propyl), $\cdot C_4H_7$ (but-3-en-1-yl), $\cdot C_4H_9$ (1-butyl) and $\cdot 2\text{-}C_4H_9$ (2-butyl)) and 10 molecules (H_2, CH_4, C_2H_2, C_2H_4, C_2H_6, C_3H_6, C_3H_8, C_4H_6 (1,3-butadiene), C_4H_8 (1-butene), C_4H_{10}) were included in the model (Table 2). Hydrocarbons larger than C_4 were neglected to keep the number of reactions tractable. Indeed, extending the network to include all reactions involving C_5 and C_6 hydrocarbons would increase the number of species from 20 to more than 250 and the number of elementary reactions to a few thousand. For such large networks,

Table 2. Calculated and Experimental Standard Enthalpies of Formation and Heat Capacities at 298 K for the 20 Species in the Ab Initio Kinetic Model

	$\Delta_f H$ (298 K), kJ/mol			C_p (298 K), J/(mol K)	
	Calculated				
Species	CBS-QB3	W1U	Exp.*	Calculated	Exp.*
·H	218.0	218.0	218.0	20.8	20.8
H_2	−5.3	−0.1	0.0	29.1	28.8
$\cdot CH_3$	147.1	144.7	147.0 ± 1.0	39.6	38.7
CH_4	−76.7	−76.3	−74.5 ± 0.4	35.7	35.7
C_2H_2	232.9	228.0	227.4 ± 0.8	43.6	44.0
$\cdot C_2H_3$	298.6	294.1	299.0 ± 5.0	44.0	–
C_2H_4	53.0	50.1	52.4 ± 0.5	43.1	42.9
$\cdot C_2H_5$	121.5	116.9	119.0 ± 2.0	51.8	–
C_2H_6	−86.0	−88.1	−83.8 ± 0.3	53.0	52.5
$\cdot C_3H_5$ (allyl)	169.0	164.3	171.0 ± 3.0	64.3	–
C_3H_6	21.2	16.2	20.4	64.8	64.3
$\cdot C_3H_7$ (1-propyl)	102.4	96.0	100.0 ± 2.0	73.1	–
$\cdot 2\text{-}C_3H_7$ (2-propyl)	89.0	83.0	90.0±2.0	68.8	
C_3H_8	−106.7	−110.6	−103.8 ± 0.6	74.5	73.6
C_4H_6 (1,3-butadiene)	114.8	107.8	111.9 ± 1.0	78.2	79.8
$\cdot C_4H_7$ (but-3-en-1-yl)	211.9	203.2	–	85.8	–
C_4H_8 (1-butene)	1.9	−4.5	−0.63 ± 0.8	88.0	85.6
$\cdot C_4H_9$ (1-butyl)	81.4	73.6	–	95.5	–
$\cdot 2\text{-}C_4H_9$ (2-butyl)	69.6	62.0	69.0 ± 2.0	92.3	
C_4H_{10}	−126.6	−132.1	−125.6 ± 0.7	100.0	98.5
Mean absolute deviation	1.9	3.8		0.8	

*Reference 40.

Table 3. Elementary Reaction Mechanism for the Steam Cracking of Ethane, Corresponding Reaction Enthalpies at 298 and 1000 K Calculated using the W1U Method, and High-Pressure Limit Rate Coefficients

		Reaction Enthalpy (kJ/mol)			Rate Coefficient [s^{-1}, m^3/(mol s) or m^6/(mol^2 s)]		
		Calculated		Exp.*		Calculated	Exp.†
	Reaction	298 K	1000 K	298 K	Calculated Arrhenius Expression	1000 K	
Radical recombination and scission reactions							
1	$\cdot CH_3 + \cdot CH_3 \rightarrow C_2H_6$	−377.5	−381.3	−378.0	$9.56 \times 10^8 T^{-0.54} \exp(-0.57[kJ/mol]/RT)$	2.14×10^7	1.77×10^7
2	$C_2H_6 \rightarrow \cdot CH_3 + \cdot CH_3$				$6.50 \times 10^{16} \exp(-369.5[kJ/mol]/RT)$	3.25×10^{-3}	4.5×10^{-3}
3	$\cdot C_2H_5 + \cdot C_2H_5 \rightarrow C_4H_{10}$	−365.9	−362.4	−363.6	$8.79 \times 10^8 T^{-0.70} \exp(0.01[kJ/mol]/RT)$	6.99×10^6	
4	$C_4H_{10} \rightarrow \cdot C_2H_5 + \cdot C_2H_5$				$4.80 \times 10^{16} \exp(-348.9[kJ/mol]/RT)$	2.86×10^{-2}	2.91×10^{-2}
5	$\cdot CH_3 + \cdot C_2H_5 \rightarrow C_3H_8$	−372.2	−373.5	−370.7	$1.21 \times 10^9 T^{-0.56} \exp(-0.09[kJ/mol]/RT)$	2.50×10^7	2.11×10^7
6	$C_3H_8 \rightarrow \cdot CH_3 + \cdot C_2H_5$				$9.50 \times 10^{16} \exp(-359.3[kJ/mol]/RT)$	1.62×10^{-2}	2.02×10^{-2}
7	$\cdot C_2H_5 + \cdot H \rightarrow C_2H_6$	−423.0	−429.8	−421.0	$5.43 \times 10^7\ T^{0.16}$	1.64×10^8	
8	$C_2H_6 \rightarrow \cdot C_2H_5 + \cdot H$				$8.80 \times 10^{16} \exp(-426.5[kJ/mol]/RT)$	4.67×10^{-6}	4.89×10^{-6}
9	$\cdot H + \cdot C_2H_3 \rightarrow C_2H_4$	−462.0	−471.7	−464.6	$3.87 \times 10^7\ T^{0.20}$	1.54×10^8	
10	$C_2H_4 \rightarrow \cdot H + \cdot C_2H_3$				$4.50 \times 10^{16} \exp(-465.0[kJ/mol]/RT)$	2.31×10^{-8}	1.74×10^{-8}
11	$\cdot C_3H_5 + \cdot H \rightarrow C_3H_6$	−366.1	−377.6	−368.6	$5.70 \times 10^7 T^{0.18} \exp(0.52[kJ/mol]/RT)$	2.10×10^8	
12	$C_3H_6 \rightarrow \cdot C_3H_5 + \cdot H$				$1.06 \times 10^{16} \exp(-370.0[kJ/mol]/RT)$	5.01×10^{-4}	
13	$\cdot H + \cdot C_3H_7 \rightarrow C_3H_8$	−424.6	−432.9	−421.8	$1.66 \times 10^7 T^{0.22}$	7.59×10^7	
14	$C_3H_8 \rightarrow \cdot H + \cdot C_3H_7$				$3.20 \times 10^{16} \exp(-425.6[kJ/mol]/RT)$	1.87×10^{-6}	
15	$\cdot CH_3 + \cdot C_2H_3 \rightarrow C_3H_6$	−421.0	−424.2	−425.6	$9.56 \times 10^8 T^{-0.54} \exp(-0.57[kJ/mol]/RT)$	2.14×10^7	
16	$C_3H_6 \rightarrow \cdot CH_3 + \cdot C_2H_3$				$3.80 \times 10^{16} \exp(-410.7[kJ/mol]/RT)$	1.34×10^{-5}	1.39×10^{-5}
17	$\cdot H + \cdot H + M \rightarrow H_2 + M$	−436.1	−444.8	−436.0	$2.97 \times 10^5 T^{-0.75}$	1.67×10^3	
18	$H_2 \rightarrow \cdot H + \cdot H$				$2.90 \times 10^{10} \exp(-422.0[kJ/mol]/RT)$	2.56×10^{-12}	
19	$\cdot C_2H_3 + \cdot C_2H_3 \rightarrow C_4H_6$	−480.3	−475.6	−486.1	$9.56 \times 10^8 T^{-0.54} \exp(-0.57[kJ/mol]/RT)$	2.14×10^7	2.00×10^7
20	$C_4H_6 \rightarrow \cdot C_2H_3 + \cdot C_2H_3$				$3.40 \times 10^{17} \exp(-464.1[kJ/mol]/RT)$	1.94×10^{-7}	
21	$\cdot C_2H_3 + \cdot C_2H_5 \rightarrow C_4H_8$	−415.5	−414.4	−418.6	$1.21 \times 10^9 T^{-0.56} \exp(-0.09[kJ/mol]/RT)$	2.50×10^7	
22	$C_4H_8 \rightarrow \cdot C_2H_3 + \cdot C_2H_5$				$9.10 \times 10^{16} \exp(-402.0[kJ/mol]/RT)$	9.11×10^{-5}	
23	$\cdot CH_3 + \cdot H \rightarrow CH_4$	−439.0	−450.4	−439.5	$6.92 \times 10^7 T^{0.18}$	2.40×10^8	2.08×10^8
24	$CH_4 \rightarrow \cdot CH_3 + \cdot H$				$3.70 \times 10^{16} \exp(-441.7[kJ/mol]/RT)$	3.15×10^{-7}	9.19×10^{-8}
25	$\cdot H + \cdot C_4H_9 \rightarrow C_4H_{10}$	−423.8	−431.9	–	$1.66 \times 10^7 T^{0.22}$	7.59×10^7	
26	$C_4H_{10} \rightarrow \cdot H + \cdot C_4H_9$				$2.90 \times 10^{16} \exp(-425.3[kJ/mol]/RT)$	1.77×10^{-6}	
27	$\cdot H + \cdot 2\text{-}C_4H_9 \rightarrow C_4H_{10}$	−412.2	−415.4	−412.6	$1.66 \times 10^7 T^{0.22}$	7.59×10^7	
28	$C_4H_{10} \rightarrow \cdot H + \cdot 2\text{-}C_4H_9$				$6.00 \times 10^{15} \exp(-409.1[kJ/mol]/RT)$	2.58×10^{-6}	
29	$\cdot H + \cdot 2\text{-}C_3H_7 \rightarrow C_3H_8$	−411.6	−417.3	−411.8	$1.66 \times 10^7 T^{0.22}$	7.59×10^7	
30	$C_3H_8 \rightarrow \cdot H + \cdot 2\text{-}C_3H_7$				$3.10 \times 10^{16} \exp(-410.8[kJ/mol]/RT)$	1.08×10^{-5}	
31	$\cdot H + \cdot C_4H_7 \rightarrow C_4H_8$	−425.8	−434.0	–	$5.70 \times 10^7 T^{0.18} \exp(0.52[kJ/mol]/RT)$	2.10×10^8	
32	$C_4H_8 \rightarrow \cdot H + \cdot C_4H_7$				$3.60 \times 10^{16} \exp(-426.6[kJ/mol]/RT)$	1.87×10^{-6}	
33	$\cdot CH_3 + \cdot C_3H_7 \rightarrow C_4H_{10}$	−372.9	−373.2	−372.6	$1.93 \times 10^8 T^{-0.32}$	2.11×10^7	
34	$C_4H_{10} \rightarrow \cdot CH_3 + \cdot C_3H_7$				$1.20 \times 10^{17} \exp(-361.0[kJ/mol]/RT)$	1.67×10^{-2}	
35	$\cdot CH_3 + \cdot C_3H_5 \rightarrow C_4H_8$	−313.6	−317.5	−318.6	$1.21 \times 10^9 T^{-0.56} \exp(-0.09[kJ/mol]/RT)$	2.50×10^7	
36	$C_4H_8 \rightarrow \cdot CH_3 + \cdot C_3H_5$				$1.50 \times 10^{16} \exp(-303.2[kJ/mol]/RT)$	2.17	
Hydrogen abstraction reactions							
37	$C_2H_6 + \cdot CH_3 \rightarrow \cdot C_2H_5 + CH_4$	−16.0	−20.6	−18.5	$3.00 \times 10^7 \exp(-69.8[kJ/mol]/RT)$	6.78×10^3	3.23×10^3
38	$CH_4 + \cdot C_2H_5 \rightarrow C_2H_6 + \cdot CH_3$				$2.00 \times 10^7 \exp(-89.0[kJ/mol]/RT)$	4.49×10^2	
39	$CH_4 + \cdot C_2H_3 \rightarrow C_2H_4 + \cdot CH_3$	−23.0	−21.3	−25.1	$2.00 \times 10^7 \exp(-61.1[kJ/mol]/RT)$	1.29×10^4	
40	$\cdot CH_3 + C_2H_4 \rightarrow CH_4 + \cdot C_2H_3$				$3.00 \times 10^7 \exp(-81.2[kJ/mol]/RT)$	1.72×10^3	
41	$C_2H_6 + \cdot H \rightarrow \cdot C_2H_5 + H_2$	−13.1	−14.9	−15.0	$4.00 \times 10^8 \exp(-50.9[kJ/mol]/RT)$	8.78×10^5	8.38×10^5
42	$\cdot C_2H_5 + H_2 \rightarrow C_2H_6 + \cdot H$				$8.00 \times 10^6 \exp(-67.0[kJ/mol]/RT)$	2.53×10^3	
43	$\cdot C_2H_3 + H_2 \rightarrow C_2H_4 + \cdot H$	−25.9	−26.9	−28.6	$5.00 \times 10^6 \exp(-39.7[kJ/mol]/RT)$	4.22×10^4	
44	$C_2H_4 + \cdot H \rightarrow H_2 + \cdot C_2H_3$				$5.00 \times 10^8 \exp(-71.1[kJ/mol]/RT)$	9.66×10^4	1.18×10^5

(*Continued*)

Table 3. (Continued)

		Reaction Enthalpy (kJ/mol)			Rate Coefficient [s^{-1}, m^3/(mol s) or m^6/(mol^2 s)]		
		Calculated		Exp.*		Calculated	Exp.†
	Reaction	298 K	1000 K	298 K	Calculated Arrhenius Expression	1000 K	
45	$\cdot CH_3 + H_2 \rightarrow CH_4 + \cdot H$	−2.9	−5.6	−3.5	$4.00 \times 10^6 \exp(-53.6[kJ/mol]/RT)$	6.34×10^3	9.63×10^3
46	$CH_4 + \cdot H \rightarrow \cdot CH_3 + H_2$				$1.00 \times 10^8 \exp(-55.7[kJ/mol]/RT)$	1.23×10^5	1.72×10^5
47	$C_4H_{10} + \cdot H \rightarrow H_2 + \cdot C_4H_9$	−12.3	−12.9	–	$4.00 \times 10^8 \exp(-58.5[kJ/mol]/RT)$	3.45×10^5	
48	$\cdot C_4H_9 + H_2 \rightarrow C_4H_{10} + \cdot H$				$5.00 \times 10^6 \exp(-71.3[kJ/mol]/RT)$	9.46×10^2	
49	$C_4H_{10} + \cdot H \rightarrow H_2 + \cdot 2\text{-}C_4H_9$	−23.9	−29.4	−23.4	$1.30 \times 10^8 \exp(-47.0[kJ/mol]/RT)$	4.58×10^5	
50	$\cdot 2\text{-}C_4H_9 + H_2 \rightarrow C_4H_{10} + \cdot H$				$8.00 \times 10^6 \exp(-76.0[kJ/mol]/RT)$	8.61×10^2	
51	$C_3H_8 + \cdot H \rightarrow H_2 + \cdot C_3H_7$	−11.5	−v11.8	−14.2	$4.20 \times 10^8 \exp(-57.5[kJ/mol]/RT)$	4.17×10^5	
52	$\cdot C_3H_7 + H_2 \rightarrow C_3H_8 + \cdot H$				$4.50 \times 10^6 \exp(-69.3[kJ/mol]/RT)$	1.08×10^3	
53	$C_3H_8 + \cdot H \rightarrow H_2 + \cdot 2\text{-}C_3H_7$	−24.5	−27.4	−24.2	$1.50 \times 10^8 \exp(-45.6[kJ/mol]/RT)$	6.19×10^5	
54	$\cdot 2\text{-}C_3H_7 + H_2 \rightarrow C_3H_8 + \cdot H$				$1.85 \times 10^6 \exp(-73.0[kJ/mol]/RT)$	2.85×10^2	
55	$C_3H_6 + \cdot H \rightarrow H_2 + \cdot C_3H_5$	−70.0	−67.1	−67.4	$1.20 \times 10^8 \exp(-43.6[kJ/mol]/RT)$	6.37×10^5	
56	$\cdot C_3H_5 + H_2 \rightarrow C_3H_6 + \cdot H$				$1.00 \times 10^7 \exp(-110.8[kJ/mol]/RT)$	1.63×10^1	
57	$C_4H_8 + \cdot H \rightarrow H_2 + \cdot C_4H_7$	−10.3	−10.7	–	$1.70 \times 10^8 \exp(-59.3[kJ/mol]/RT)$	1.36×10^5	
58	$\cdot C_4H_7 + H_2 \rightarrow C_4H_8 + \cdot H$				$4.30 \times 10^6 \exp(-70.0[kJ/mol]/RT)$	9.54×10^2	
59	$\cdot CH_3 + C_4H_{10} \rightarrow CH_4 + \cdot C_4H_9$	−15.2	−18.5	–	$3.00 \times 10^7 \exp(-82.2[kJ/mol]/RT)$	1.53×10^3	
60	$CH_4 + \cdot C_4H_9 \rightarrow C_4H_{10} + \cdot CH_3$				$1.30 \times 10^7 \exp(-98.9[kJ/mol]/RT)$	8.92×10^1	
61	$\cdot CH_3 + C_4H_{10} \rightarrow CH_4 + \cdot 2\text{-}C_4H_9$	−26.8	−35.0	−26.9	$1.40 \times 10^7 \exp(-70.8[kJ/mol]/RT)$	2.81×10^3	
62	$CH_4 + \cdot 2\text{-}C_4H_9 \rightarrow C_4H_{10} + \cdot CH_3$				$3.00 \times 10^7 \exp(-103.7[kJ/mol]/RT)$	1.15×10^2	
63	$\cdot CH_3 + C_3H_8 \rightarrow CH_4 + \cdot C_3H_7$	−14.4	−17.5	−17.7	$2.80 \times 10^7 \exp(-80.1[kJ/mol]/RT)$	1.83×10^3	
64	$CH_4 + \cdot C_3H_7 \rightarrow C_3H_8 + \cdot CH_3$				$1.00 \times 10^7 \exp(-95.8[kJ/mol]/RT)$	9.93×10^1	
65	$\cdot CH_3 + C_3H_8 \rightarrow CH_4 + \cdot 2\text{-}C_3H_7$	−27.4	−33.0	−27.7	$1.80 \times 10^7 \exp(-69.9[kJ/mol]/RT)$	4.01×10^3	
66	$CH_4 + \cdot 2\text{-}C_3H_7 \rightarrow C_3H_8 + \cdot CH_3$				$7.10 \times 10^6 \exp(-101.1[kJ/mol]/RT)$	3.72×10^1	
67	$\cdot CH_3 + C_3H_6 \rightarrow CH_4 + \cdot C_3H_5$	−72.9	−72.8	−70.9	$3.20 \times 10^7 \exp(-57.5[kJ/mol]/RT)$	3.19×10^4	
68	$CH_4 + \cdot C_3H_5 \rightarrow C_3H_6 + \cdot CH_3$				$9.00 \times 10^7 \exp(-128.6[kJ/mol]/RT)$	1.72×10^1	
69	$\cdot CH_3 + C_4H_8 \rightarrow CH_4 + \cdot C_4H_7$	−13.2	−16.3	–	$1.20 \times 10^7 \exp(-80.8[kJ/mol]/RT)$	7.19×10^2	
70	$CH_4 + \cdot C_4H_7 \rightarrow C_4H_8 + \cdot CH_3$				$1.00 \times 10^7 \exp(-95.4[kJ/mol]/RT)$	1.04×10^2	
71	$C_2H_6 + \cdot C_2H_3 \rightarrow C_2H_4 + \cdot C_2H_5$	−39.0	−41.9	−43.8	$2.40 \times 10^7 \exp(-49.6[kJ/mol]/RT)$	6.17×10^4	
72	$C_2H_4 + \cdot C_2H_5 \rightarrow C_2H_6 + \cdot C_2H_3$				$1.30 \times 10^7 \exp(-87.8[kJ/mol]/RT)$	3.37×10^2	
73	$C_2H_6 + \cdot C_4H_9 \rightarrow C_4H_{10} + \cdot C_2H_5$	−0.8	−2.1	–	$1.15 \times 10^7 \exp(-79.0[kJ/mol]/RT)$	8.62×10^2	2.61×10^2
74	$C_4H_{10} + \cdot C_2H_5 \rightarrow C_2H_6 + \cdot C_4H_9$				$8.00 \times 10^6 \exp(-77.4[kJ/mol]/RT)$	7.28×10^2	
75	$C_4H_{10} + \cdot C_2H_5 \rightarrow C_2H_6 + \cdot 2\text{-}C_4H_9$	−10.8	−14.4	−8.2	$7.00 \times 10^6 \exp(-79.4[kJ/mol]/RT)$	4.99×10^2	
76	$C_2H_6 + \cdot 2\text{-}C_4H_9 \rightarrow C_4H_{10} + \cdot C_2H_5$				$5.00 \times 10^7 \exp(-97.2[kJ/mol]/RT)$	4.19×10^2	
77	$C_2H_6 + \cdot C_3H_7 \rightarrow C_3H_8 + \cdot C_2H_5$	−1.7	−3.1	−1.0	$9.60 \times 10^6 \exp(-76.8[kJ/mol]/RT)$	9.36×10^2	
78	$C_3H_8 + \cdot C_2H_5 \rightarrow C_2H_6 + \cdot C_3H_7$				$7.70 \times 10^6 \exp(-76.2[kJ/mol]/RT)$	8.06×10^2	
79	$C_3H_8 + \cdot C_2H_5 \rightarrow C_2H_6 + \cdot 2\text{-}C_3H_7$	−11.4	−12.5	−9.0	$9.70 \times 10^7 \exp(-79.1[kJ/mol]/RT)$	7.14×10^2	
80	$C_2H_6 + \cdot 2\text{-}C_3H_7 \rightarrow C_3H_8 + \cdot C_2H_5$				$1.40 \times 10^7 \exp(-95.3[kJ/mol]/RT)$	1.48×10^2	
81	$C_3H_6 + \cdot C_2H_5 \rightarrow C_2H_6 + \cdot C_3H_5$	−56.9	−52.2	−52.2	$1.50 \times 10^7 \exp(-70.2[kJ/mol]/RT)$	3.22×10^3	
82	$C_2H_6 + \cdot C_3H_5 \rightarrow C_3H_6 + \cdot C_2H_5$				$1.50 \times 10^8 \exp(-126.4[kJ/mol]/RT)$	3.76×10^1	
83	$C_2H_6 + \cdot C_4H_7 \rightarrow C_4H_8 + \cdot C_2H_5$	−2.8	−4.2	–	$1.10 \times 10^7 \exp(-76.5[kJ/mol]/RT)$	1.12×10^3	
84	$C_4H_8 + \cdot C_2H_5 \rightarrow C_2H_6 + \cdot C_4H_7$				$3.60 \times 10^6 \exp(-77.0[kJ/mol]/RT)$	3.43×10^2	
85	$C_4H_{10} + \cdot C_2H_3 \rightarrow C_2H_4 + \cdot C_4H_9$	−38.2	−39.8	–	$1.90 \times 10^7 \exp(-60.9[kJ/mol]/RT)$	1.26×10^4	
86	$C_2H_4 + \cdot C_4H_9 \rightarrow C_4H_{10} + \cdot C_2H_3$				$1.50 \times 10^7 \exp(-100.7[kJ/mol]/RT)$	8.26×10^1	
87	$C_4H_{10} + \cdot C_2H_3 \rightarrow C_2H_4 + \cdot 2\text{-}C_4H_9$	−49.8	−56.3	−52.0	$1.30 \times 10^7 \exp(-51.5[kJ/mol]/RT)$	2.66×10^4	
88	$C_2H_4 + \cdot 2\text{-}C_4H_9 \rightarrow C_4H_{10} + \cdot C_2H_3$				$5.00 \times 10^7 \exp(-107.5[kJ/mol]/RT)$	1.21×10^2	
89	$C_3H_8 + \cdot C_2H_3 \rightarrow C_2H_4 + \cdot C_3H_7$	−37.4	−38.8	−42.8	$2.80 \times 10^7 \exp(-59.3[kJ/mol]/RT)$	2.24×10^4	
90	$C_2H_4 + \cdot C_3H_7 \rightarrow C_3H_8 + \cdot C_2H_3$				$1.80 \times 10^7 \exp(-98.1[kJ/mol]/RT)$	1.35×10^2	
91	$C_3H_8 + \cdot C_2H_3 \rightarrow C_2H_4 + \cdot 2\text{-}C_3H_7$	−50.4	−54.3	−52.8	$1.30 \times 10^7 \exp(-50.1[kJ/mol]/RT)$	3.13×10^4	

(*Continued*)

Table 3. (Continued)

		Reaction Enthalpy (kJ/mol)			Rate Coefficient [s^{-1}, m^3/(mol s) or m^6/(mol^2 s)]		
		Calculated		Exp.*		Calculated	Exp.†
	Reaction	298 K	1000 K	298 K	Calculated Arrhenius Expression	1000 K	
92	$C_2H_4 + \cdot 2\text{-}C_3H_7 \rightarrow C_3H_8 + \cdot C_2H_3$				$9.50 \times 10^6 \exp(-104.5[kJ/mol]/RT)$	3.30×10^1	
93	$C_3H_6 + \cdot C_2H_3 \rightarrow C_2H_4 + \cdot C_3H_5$	−95.9	−94.1	−96.0	$1.60 \times 10^7 \exp(-46.1[kJ/mol]/RT)$	6.28×10^4	
94	$C_2H_4 + \cdot C_3H_5 \rightarrow C_3H_6 + \cdot C_2H_3$				$8.00 \times 10^7 \exp(-140.4[kJ/mol]/RT)$	3.70	
95	$C_4H_8 + \cdot C_2H_3 \rightarrow C_2H_4 + \cdot C_4H_7$	−36.2	−37.7	–	$8.50 \times 10^6 \exp(-60.4[kJ/mol]/RT)$	5.98×10^3	
96	$C_2H_4 + \cdot C_4H_7 \rightarrow C_4H_8 + \cdot C_2H_3$				$1.30 \times 10^7 \exp(-98.0[kJ/mol]/RT)$	9.85×10^1	
97	$C_4H_{10} + \cdot C_3H_7 \rightarrow C_3H_8 + \cdot C_4H_9$	−0.9	−1.0	–	$1.40 \times 10^7 \exp(-93.4[kJ/mol]/RT)$	1.86×10^2	
98	$C_3H_8 + \cdot C_4H_9 \rightarrow C_4H_{10} + \cdot C_3H_7$				$1.70 \times 10^7 \exp(-94.4[kJ/mol]/RT)$	2.00×10^2	
99	$C_4H_{10} + \cdot 2\text{-}C_3H_7 \rightarrow C_3H_8 + \cdot C_4H_9$	12.1	14.6	–	$8.70 \times 10^6 \exp(-83.6[kJ/mol]/RT)$	3.72×10^2	
100	$C_3H_8 + \cdot C_4H_9 \rightarrow C_4H_{10} + \cdot 2\text{-}C_3H_7$				$9.10 \times 10^6 \exp(-69.1[kJ/mol]/RT)$	2.23×10^3	
101	$C_3H_6 + \cdot C_4H_9 \rightarrow C_4H_{10} + \cdot C_3H_5$	−57.7	−54.3	–	$9.50 \times 10^6 \exp(-63.9[kJ/mol]/RT)$	4.36×10^3	
102	$C_4H_{10} + \cdot C_3H_5 \rightarrow C_3H_6 + \cdot C_4H_9$				$6.60 \times 10^7 \exp(-118.4[kJ/mol]/RT)$	4.32×10^1	
103	$C_4H_{10} + \cdot C_4H_7 \rightarrow C_4H_8 + \cdot C_4H_9$	−2.0	−2.1	–	$1.40 \times 10^7 \exp(-92.5[kJ/mol]/RT)$	2.07×10^2	
104	$C_4H_8 + \cdot C_4H_9 \rightarrow C_4H_{10} + \cdot C_4H_7$				$7.00 \times 10^6 \exp(-94.6[kJ/mol]/RT)$	8.00×10^1	
105	$C_4H_{10} + \cdot C_3H_7 \rightarrow C_3H_8 + \cdot 2\text{-}C_4H_9$	−12.4	−17.5	−9.2	$6.50 \times 10^6 \exp(-81.4[kJ/mol]/RT)$	3.62×10^2	
106	$C_3H_8 + \cdot 2\text{-}C_4H_9 \rightarrow C_4H_{10} + \cdot C_3H_7$				$3.80 \times 10^7 \exp(-98.7[kJ/mol]/RT)$	2.66×10^2	
107	$C_4H_{10} + \cdot 2\text{-}C_3H_7 \rightarrow C_3H_8 + \cdot 2\text{-}C_4H_9$	7.5	−2.0	0.8	$2.70 \times 10^6 \exp(-70.7[kJ/mol]/RT)$	5.46×10^2	
108	$C_3H_8 + \cdot 2\text{-}C_4H_9 \rightarrow C_4H_{10} + \cdot 2\text{-}C_3H_7$				$1.40 \times 10^7 \exp(-72.4[kJ/mol]/RT)$	2.31×10^3	
109	$C_3H_6 + \cdot 2\text{-}C_4H_9 \rightarrow C_4H_{10} + \cdot C_3H_5$	−46.1	−37.8	−44.0	$1.90 \times 10^8 \exp(-71.2[kJ/mol]/RT)$	3.61×10^4	
110	$C_4H_{10} + \cdot C_3H_5 \rightarrow C_3H_6 + \cdot 2\text{-}C_4H_9$				$2.70 \times 10^8 \exp(-109.5[kJ/mol]/RT)$	5.15×10^2	
111	$C_4H_{10} + \cdot C_4H_7 \rightarrow C_4H_8 + \cdot 2\text{-}C_4H_9$	−13.6	−18.6	–	$7.00 \times 10^6 \exp(-81.0[kJ/mol]/RT)$	4.13×10^2	
112	$C_4H_8 + \cdot 2\text{-}C_4H_9 \rightarrow C_4H_{10} + \cdot C_4H_7$				$1.70 \times 10^7 \exp(-99.4[kJ/mol]/RT)$	1.10×10^2	
113	$C_3H_6 + \cdot C_3H_7 \rightarrow C_3H_8 + \cdot C_3H_5$	−58.8	−55.5	−53.2	$4.10 \times 10^6 \exp(-71.3[kJ/mol]/RT)$	7.78×10^2	
114	$C_3H_8 + \cdot C_3H_5 \rightarrow C_3H_6 + \cdot C_3H_7$				$3.50 \times 10^7 \exp(-127.0[kJ/mol]/RT)$	8.09	
115	$C_3H_8 + \cdot C_4H_7 \rightarrow C_4H_8 + \cdot C_3H_7$	−1.1	−1.1	–	$1.25 \times 10^7 \exp(-79.2[kJ/mol]/RT)$	9.09×10^2	
116	$C_4H_8 + \cdot C_3H_7 \rightarrow C_3H_8 + \cdot C_4H_7$				$5.20 \times 10^6 \exp(-80.3[kJ/mol]/RT)$	3.31×10^2	
117	$C_3H_6 + \cdot 2\text{-}C_3H_7 \rightarrow C_3H_8 + \cdot C_3H_5$	−45.5	−39.7	−43.2	$3.50 \times 10^6 \exp(-63.5[kJ/mol]/RT)$	1.68×10^3	
118	$C_3H_8 + \cdot C_3H_5 \rightarrow C_3H_6 + \cdot 2\text{-}C_3H_7$				$2.50 \times 10^7 \exp(-103.5[kJ/mol]/RT)$	9.79×10^1	
119	$C_3H_6 + \cdot C_4H_7 \rightarrow C_4H_8 + \cdot C_3H_5$	−59.7	−56.4	–	$7.00 \times 10^6 \exp(-61.8[kJ/mol]/RT)$	4.12×10^3	
120	$C_4H_8 + \cdot C_3H_5 \rightarrow C_3H_6 + \cdot C_4H_7$				$2.40 \times 10^7 \exp(-118.5[kJ/mol]/RT)$	1.55×10^1	
121	$C_3H_8 + \cdot C_4H_7 \rightarrow C_4H_8 + \cdot 2\text{-}C_3H_7$	−14.1	−16.7	–	$8.50 \times 10^6 \exp(-80.4[kJ/mol]/RT)$	5.39×10^2	
122	$C_4H_8 + \cdot 2\text{-}C_3H_7 \rightarrow C_3H_8 + \cdot C_4H_7$				$4.00 \times 10^6 \exp(-97.0[kJ/mol]/RT)$	3.42×10^1	
Radical addition and β-scission reactions							
123	$C_2H_4 + \cdot H \rightarrow \cdot C_2H_5$	−151.2	−156.0	−151.4	$1.00 \times 10^8 \exp(-17.2[kJ/mol]/RT)$	1.26×10^7	
124	$\cdot C_2H_5 \rightarrow C_2H_4 + \cdot H$				$5.70 \times 10^{13} \exp(-166.6[kJ/mol]/RT)$	1.13×10^5	5.67×10^4
125	$\cdot C_2H_5 + C_2H_4 \rightarrow \cdot C_4H_9$	−93.3	−88.0	–	$1.18 \times 10^5 \exp(-31.9[kJ/mol]/RT)$	2.54×10^3	5.58×10^3
126	$\cdot C_4H_9 \rightarrow \cdot C_2H_5 + C_2H_4$				$3.00 \times 10^{12} \exp(-112.4[kJ/mol]/RT)$	4.05×10^6	4.17×10^6
127	$\cdot CH_3 + C_2H_4 \rightarrow \cdot C_3H_7$	−98.8	−97.1	−99.4	$2.00 \times 10^6 \exp(-41.7[kJ/mol]/RT)$	1.33×10^4	
128	$\cdot C_3H_7 \rightarrow \cdot CH_3 + C_2H_4$				$2.00 \times 10^{13} \exp(-130.3[kJ/mol]/RT)$	3.13×10^6	
129	$\cdot C_2H_3 + C_2H_4 \rightarrow \cdot C_4H_7$	−140.9	−136.8	–	$9.21 \times 10^5 \exp(-19.0[kJ/mol]/RT)$	9.37×10^4	
130	$\cdot C_4H_7 \rightarrow \cdot C_2H_3 + C_2H_4$				$2.10 \times 10^{13} \exp(-149.2[kJ/mol]/RT)$	3.38×10^5	
131	$C_2H_2 + \cdot H \rightarrow \cdot C_2H_3$	−151.9	−161.8	−145.7	$4.00 \times 10^8 \exp(-21.2[kJ/mol]/RT)$	3.12×10^7	1.79×10^7
132	$\cdot C_2H_3 \rightarrow C_2H_2 + \cdot H$				$2.70 \times 10^{14} \exp(-174.3[kJ/mol]/RT)$	2.14×10^5	2.34×10^5
133	$\cdot CH_3 + C_2H_2 \rightarrow \cdot C_3H_5$	−208.4	−212.1	−203.4	$1.00 \times 10^7 \exp(-39.2[kJ/mol]/RT)$	8.96×10^4	
134	$\cdot C_3H_5 \rightarrow C_2H_2 + \cdot CH_3$				$4.20 \times 10^{14} \exp(-239.2[kJ/mol]/RT)$	1.34×10^2	
135	$C_3H_6 + \cdot H \rightarrow \cdot C_3H_7$	−138.2	−142.9	−138.4	$2.00 \times 10^7 \exp(-20.3[kJ/mol]/RT)$	1.74×10^6	
136	$\cdot C_3H_7 \rightarrow C_3H_6 + \cdot H$				$1.70 \times 10^{13} \exp(-156.2[kJ/mol]/RT)$	1.17×10^5	
137	$C_4H_6 + \cdot H \rightarrow \cdot C_4H_7$	−122.6	−132.5	–	$3.00 \times 10^7 \exp(-18.6[kJ/mol]/RT)$	3.20×10^6	

(*Continued*)

Table 3. (Continued)

	Reaction	Reaction Enthalpy (kJ/mol)			Rate Coefficient [s^{-1}, m^3/(mol s) or m^6/(mol^2 s)]		
		Calculated		Exp.*		Calculated	Exp.†
		298 K	1000 K	298 K	Calculated Arrhenius Expression	1000 K	
138	$\cdot C_4H_7 \rightarrow C_4H_6 + \cdot H$				$6.40 \times 10^{12}\exp(-144.2[kJ/mol]/RT)$	1.87×10^5	
139	$C_4H_8 + \cdot H \rightarrow \cdot C_4H_9$	−139.8	−144.2	–	$6.00 \times 10^6\exp(-16.1[kJ/mol]/RT)$	8.65×10^5	
140	$\cdot C_4H_9 \rightarrow C_4H_8 + \cdot H$				$5.80 \times 10^{12}\exp(-153.5[kJ/mol]/RT)$	5.57×10^4	1.83×10^5
141	$C_3H_6 + \cdot H \rightarrow \cdot 2\text{-}C_3H_7$	−151.2	−159.8	−148.4	$6.00 \times 10^7\exp(-12.9[kJ/mol]/RT)$	1.27×10^7	
142	$\cdot 2\text{-}C_3H_7 \rightarrow C_3H_6 + \cdot H$				$5.90 \times 10^{13}\exp(-164.4[kJ/mol]/RT)$	1.53×10^5	
143	$C_4H_8 + \cdot H \rightarrow \cdot 2\text{-}C_4H_9$	−151.4	−162.1	−148.4	$1.30 \times 10^7\exp(-13.5[kJ/mol]/RT)$	2.57×10^6	
144	$\cdot 2\text{-}C_4H_9 \rightarrow C_4H_8 + \cdot H$				$6.30 \times 10^{13}\exp(-167.1[kJ/mol]/RT)$	1.18×10^5	
145	$\cdot CH_3 + C_3H_6 \rightarrow \cdot 2\text{-}C_4H_9$	−98.9	−102.0	−98.4	$1.15 \times 10^6\exp(-35.7[kJ/mol]/RT)$	1.57×10^4	3.21×10^4
146	$\cdot 2\text{-}C_4H_9 \rightarrow C_3H_6 + \cdot CH_3$				$1.25 \times 10^{14}\exp(-127.9[kJ/mol]/RT)$	2.61×10^7	8.85×10^6
Isomerization reactions							
147	$\cdot C_3H_7 \rightarrow \cdot 2\text{-}C_3H_7$	−13.0	−15.6	−10.0	$5.80 \times 10^{12}\exp(-155.0[kJ/mol]/RT)$	4.61×10^4	
148	$\cdot 2\text{-}C_3H_7 \rightarrow \cdot C_3H_7$				$6.60 \times 10^{12}\exp(-170.6[kJ/mol]/RT)$	8.09×10^3	
149	$\cdot C_4H_9 \rightarrow \cdot 2\text{-}C_4H_9$	−11.6	−16.5		$4.70 \times 10^{12}\exp(-154.8[kJ/mol]/RT)$	3.80×10^4	
150	$\cdot 2\text{-}C_4H_9 \rightarrow \cdot C_4H_9$				$2.10 \times 10^{13}\exp(-170.4[kJ/mol]/RT)$	2.63×10^4	
Mean absolute deviation‡		2.4				1.7	

*Reference 40.
†Reference 41.
‡For the rate coefficients, the mean absolute ratio was calculated.

automated network generation algorithms[12,13,15,27] become required to ensure that all possible reactions are included. The 150 reactions in our reaction network include 18 radical-radical recombination and 18 corresponding bond scission reactions; 12 radical addition and 12 corresponding β-scission reactions; 86 hydrogen abstraction reactions and 4 radical isomerization reactions (Table 3). All possible reactions in these three families involving the 20 species were included in the reaction network.

Though steam cracking proceeds via a radical mechanism, elementary molecular reactions have been suggested to play an important role in steam cracking.[16] To evaluate the importance of such reactions for our conditions, we calculated the rate coefficient for the direct C_2H_6 decomposition to C_2H_4 and H_2. At 1000 K, the rate coefficient of 9.65×10^{-12} s^{-1} is much smaller than the rate coefficient for C_2H_6 decomposition to $\cdot CH_3$ radicals, 3.25×10^{-3} s^{-1} (Table 3), which is again smaller than the typical rate of hydrogen abstraction, $\cdot R + C_2H_6$, of 1.57×10^{-2} s^{-1} at those conditions and for typical radical concentrations. This is consistent with an early study by Benson and Haugen.[42] Next, we evaluated the rate for C_2H_4 consumption by a direct molecular reaction with H_2. The rate for this reaction, 3.29×10^{-13} s^{-1} at 1000 K and for typical H_2 concentrations, is much smaller than the rate for radical addition by $\cdot H$ and $\cdot CH_3$ radicals, 1.46×10^1 and 3.08×10^{-2} s^{-1}, at typical conditions and radical concentrations. The rate of C_2H_4 consumption by a Diels Alder reaction with C_4H_6, 1.49×10^{-3} s^{-1}, is also too small to contribute to the consumption of C_2H_4. These elementary molecular reactions can hence be safely neglected in our ab initio kinetic model.

Ab initio calculation of thermodynamic and kinetic parameters

Standard enthalpies of formation were calculated using the Complete Basis Set CBS-QB3 method[29,30] and the Weizmann W1U method[28] as implemented in the Gaussian03 package.[43] The CBS-QB3 method was developed to reach so-called chemical accuracy, i.e., an average accuracy of 1 kcal/mol,[29,30] while the Weizmann W1 method was developed to compute thermochemical properties of small molecules with an average 1 kJ/mol accuracy.[28] Entropies and heat capacities were computed from CBS-QB3 geometries and vibration frequencies using standard formulas from statistical mechanics.[44] Internal rotation partition functions were obtained using the one-dimensional hindered rotor approximation,[21] and rotational potentials were calculated at the B3LYP/6-311G(d,p) level of theory. A 0.9679 scaling factor[45] was used for frequencies that enter the vibration partition functions, while Zero Point Energies (ZPE) were taken from the CBS-QB3 and W1U results.

Rate coefficients for hydrogen abstraction reactions were calculated using the microscopic formulation of transition state theory:

$$k(T) = \kappa(T)\frac{k_B T}{c_0 h}\frac{Q_{TS}(T)}{Q_R(T)}e^{\left(\frac{-\Delta E_0(0K)}{RT}\right)} \quad (1)$$

where k_B is the Boltzmann constant, h is the Planck constant, c_0 is the concentration in the standard state to which the translational partition function is referred, and $Q_R(T)$ and

$Q_{TS}(T)$ are the reactant and transition state partition functions, respectively. Rotational symmetry numbers for the reactants and the transition state are included in the partition functions and account for the reaction path degeneracy.[46] The activation barrier at 0 K, ΔE_0(0 K), is the energy difference between the transition state and the reactants at 0 K, including the ZPE, and was calculated with the CBS-QB3 method. The tunneling correction factor $\kappa(T)$ accounts for the effect of quantum mechanical tunneling on the reaction rate. Tunneling corrections were calculated using the Eckart method.[33,47] All transition states were first order saddle points with a single large amplitude imaginary frequency. Following the reaction path by integrating the intrinsic reaction coordinate (IRC) for a typical hydrogen abstraction reaction, $C_2H_6 + \cdot CH_3 \rightarrow \cdot C_2H_5 + CH_4$, confirmed that the reactants and the products are connected through a single transition state for this family of reactions. For the 43 pairs of hydrogen abstraction reactions, only the rate coefficient for the exothermic reaction of each pair was calculated using transition state theory. The rate coefficient for the corresponding reverse endothermic reaction was calculated by combining the forward rate coefficient with the equilibrium coefficient calculated using either the CBS-QB3 or the W1U reaction energy. This approach ensures that the kinetic parameters remain thermodynamically consistent when W1U enthalpies of formation are used.

Rate coefficients for radical addition reactions were calculated using canonical variational transition state theory (CVT) as implemented in the Polyrate9.7[48] and Gaussrate9.7[49] programs. In CVT, the transition state is located at the Gibbs free energy maximum along the minimum energy path (MEP) reaction coordinate s rather than at the potential energy maximum (Eq. 2). CVT hence incorporates entropic effects into the location of the transition state.[50]

$$k_{CVT}(T) = \min_s k(T,s) \tag{2}$$

The free energy profile along the MEP was computed using the CBS-QB3 method. In particular for potential energy surfaces that are rather flat near the transition state and at high temperatures, the use of CVT instead of conventional TST becomes important.[51,52] Tunneling corrections were again included using the Eckart method, but are small for this family of reactions. All transition states were characterized by a single large amplitude imaginary frequency. Following the IRC led to the expected reactants and products for all reactions. For the addition of a ·H radical to C_3H_6, $\cdot H + C_3H_6 \rightarrow \cdot 2\text{-}C_3H_7$, and to 1-butene, $\cdot H + C_4H_8 \rightarrow \cdot 2\text{-}C_4H_9$, the geometries and vibration frequencies along the MEP were calculated at the MPW1K/6-311G(d,p) level of theory because the B3LYP/6-311G(d,p) level of theory which is used in the CBS-QB3 method fails to identify the transition states for these two reactions.[31] Rate coefficients for the reverse β-scission reactions were calculated by combining the corresponding radical addition rate coefficient with the equilibrium coefficient calculated using either the CBS-QB3 or the W1U method. Rate coefficients for the $\cdot C_3H_7$ and $\cdot C_4H_9$ isomerization reactions were calculated following the procedure described for radical addition reactions.

Finally, rate coefficients for 9 of the 18 radical recombination reactions were obtained from ab initio calculations by Klippenstein et al.[37,38] In their work, the potential energy surface that describes the interaction between the reactant radicals is calculated using complete-active-space second order perturbation theory (CASPT2/cc-pvdz) and the rate coefficients are computed using VRC-TST. The resulting rate coefficients show good agreement with experimental data.[37,38] Unfortunately, Klippenstein et al. did not report rate coefficients for reactions involving the $\cdot C_2H_3$ radical, i.e., $\cdot CH_3 + \cdot C_2H_3 \rightarrow C_3H_6$, $\cdot C_2H_3 + \cdot C_2H_3 \rightarrow C_4H_6$ and $\cdot C_2H_3 + \cdot C_2H_5 \rightarrow C_4H_8$ in our model, for some of the reactions involving ·H, i.e., $\cdot C_4H_9 + \cdot H \rightarrow C_4H_{10}$, $\cdot 2\text{-}C_4H_9 + \cdot H \rightarrow C_4H_{10}$, $\cdot 2\text{-}C_3H_7 + \cdot H \rightarrow C_3H_8$, and $\cdot C_4H_7 + \cdot H \rightarrow C_4H_8$ in our model, or for $\cdot C_3H_5 + \cdot CH_3 \rightarrow C_4H_8$. Because of the relative small difference between rate coefficients involving $\cdot C_2H_5$ and $\cdot CH_3$ radicals, i.e., typically less than a factor 1.5, we used the $\cdot CH_3$ rate coefficients for reactions involving $\cdot C_2H_3$ radicals. Due to the similarity between the $\cdot C_3H_7$ radical and the $\cdot C_4H_9$, $\cdot 2\text{-}C_4H_9$, $\cdot 2\text{-}C_3H_7$, and $\cdot C_4H_7$ radicals, the rate coefficient for the $\cdot C_3H_7 + \cdot H \rightarrow C_3H_8$ reaction was also used for recombination reactions of the ·H radical with $\cdot C_4H_9$, $\cdot 2\text{-}C_4H_9$, $\cdot 2\text{-}C_3H_7$, and $\cdot C_4H_7$. Finally, the rate coefficient for the $\cdot CH_3 + \cdot C_2H_5 \rightarrow C_3H_8$ reaction was used for the $\cdot CH_3 + \cdot C_3H_5 \rightarrow C_4H_8$ reaction. Recombination of two ·H radicals requires a third body to stabilize the H_2 product.[53] Hence for the reaction $\cdot H + \cdot H + M \rightarrow H_2 + M$ we used the third order rate coefficient calculated by Schwenke[54] with an ab initio based Master Equation approach in our model. Rate coefficients for the reverse scission reactions were calculated by combining the forward recombination rate coefficients with equilibrium coefficients calculated using the CBS-QB3 or the W1U method. Sensitivity analysis shows that the yields of the major products C_2H_6, C_2H_4, H_2, CH_4, C_3H_6, and C_2H_2 are not sensitive to the values of the eight recombination rate coefficients for which no direct ab initio data were available. Indeed, the normalized yield change coefficients (Eq. 3) for these reactions are all less than 0.03, indicating that changing the rate coefficients by a factor two changes the simulated yields by less than 3%.

All the calculated forward and reverse rate coefficients are reported in an Arrhenius form in Table 3. The reverse rate coefficients in Table 3 were calculated using the W1U equilibrium coefficients. The Arrhenius parameters were obtained by fitting to calculated rate coefficients between 800 and 1200 K. All the calculated rate coefficients except the $\cdot H + \cdot H$ recombination rate coefficient correspond to the high-pressure limit. However, at typical ethane steam cracking temperatures and pressure, some of the rate coefficients in our reaction network may be in the fall-off regime even above 1 atm.[8]

The effect of the total pressure on each of the rate coefficients was therefore evaluated at 1000 K and 2.5 atm using the three-frequency version of Quantum Rice-Ramsberger-Kassel theory[55] with the Modified Strong-Collision approximation (QRRK-MSC)[56] as implemented in CHEMDIS.[57] H_2O was used as the bath gas.

Experimental conditions

To evaluate the accuracy of the ab initio kinetic model, conversions and yields were simulated for three experimental

conditions (Table 1). The process conditions and experimental yields were taken from Froment et al.[2,3] and from Wauters.[39] The first set of data corresponds to an industrial ethane cracker with an ethane conversion of 59.9% and a residence time of 0.93 s.[3] The feed consists of 98.2 mol % C_2H_6, 1.0 mol % C_2H_4, and 0.8 mol % C_3H_6. The average heat flux was not reported by Froment et al.,[3] but can be estimated from an overall energy balance. Based on the reported inlet and outlet compositions, flowrate and temperatures, the reactor geometry, and the ab initio enthalpies of formation in Table 2, an average heat flux of 63.1 kW/m^2 was calculated. The second set of data is for a pilot-scale reactor with a similar conversion and a residence time of 0.64 s.[2] The average heat flux of 5.6 kW/m^2 was again estimated from an overall energy balance. The third dataset corresponds to an industrial ethane cracker with a split coil reactor with a diameter of 0.124 m for the first 76 m, and a larger 0.136 m diameter for the remaining 25 m. The conversion for the third case is 51.1%, and the residence time is 1.2 s. The feed consists of 98.0 mol % C_2H_6, 1.0 mol % C_2H_4, and 1.0 mol % C_3H_6. An average heat flux of 75.4 kW/m^2 was estimated. The material, energy and momentum equations were simulated for a one-dimensional ideal plug flow reactor (PFR).[3] Simulations by Van Geem et al.[6] indicate that this is a good approximation, though the radial temperature gradient might be somewhat underestimated.

Sensitivity analysis

Sensitivity analysis was used to help identify the rate coefficients that affect the yields of the major products most. Similar to the sensitivity coefficient in a local sensitivity analysis,[58] a normalized yield change coefficient λ_{ij} was calculated for the products C_2H_6, C_2H_4, CH_4, H_2, C_3H_6, and C_2H_2:

$$\lambda_{ij} = \frac{k_j}{W_i}\frac{\Delta W_i}{\Delta k_j} \tag{3}$$

where W_i is the yield of species i and k_j is the rate coefficient for reaction j. To maintain thermodynamic consistency, both the forward and reverse rate coefficients were multiplied by the same factor.

Results and Discussion

Thermodynamic properties for the 20 species included in the reaction network and rate coefficients for the 150 elementary reactions are discussed first. Next, steam cracking of ethane is simulated for the three cases summarized in Table 1, using the ab initio kinetic and thermodynamic parameters. The importance of the pressure dependence of the rate coefficients is evaluated next. Finally, the sensitivity of the simulated yields to the calculated kinetic parameters is discussed.

Thermodynamic and kinetic parameters

Calculated enthalpies of formation and heat capacities for the 20 species in the kinetic model are presented in Table 2. For the enthalpies of formation at 298 K, the mean absolute deviation (MAD) with available experimental data is 1.9 and 3.8 kJ/mol for the CBS-QB3 and W1U method, respectively. One should note that the average experimental uncertainty for the 18 enthalpies of formation is 1.4 kJ/mol, with a maximum of 5.0 kJ/mol for the $\cdot C_2H_3$ radical. Our results are comparable to more detailed benchmark studies of the CBS-QB3 method,[23,29,30] and empirical bond additive correction schemes have been proposed to further improve the accuracy.[23,31] To avoid introducing experimental data into our simulations, we have however opted to use the CBS-QB3 data without empirical corrections. Based on extensive benchmark studies of the accuracy of the W1 method for the calculation of atomization energies of small first and second row molecules, a MAD of 1.3 kJ/mol has been reported.[28] The larger MAD for the W1U enthalpies of formation in our small hydrocarbon set can be mainly attributed to deviations for larger molecules in the set, again consistent with literature data.[59] Indeed, deviations with experimental data tend to increase with the number of carbon atoms in the molecule for both the CBS-QB3 and the W1U method, and for each additional carbon atom in the molecule the difference between the W1U and CBS-QB3 enthalpies of formation increases by about 2 kJ/mol. However, the W1U method is more accurate for the six main products in our model, H_2, CH_4, C_2H_2, C_2H_4, C_2H_6, and C_3H_6, with a MAD of 2.2 kJ/mol compared to 2.8 kJ/mol for the CBS-QB3 method, and the deviations are rather uniform. Consequently, deviations between W1U and experimental reaction enthalpies for the important $C_2H_6 \rightarrow C_2H_4 + H_2$, $C_2H_6 \rightarrow 2\ \cdot CH_3$, and $C_2H_6 + H_2 \rightarrow 2\ CH_4$ overall reactions are only -1.9, $+0.5$ and $+0.8$ kJ/mol, respectively, while the CBS-QB3 enthalpies show slightly larger deviations of $+2.5$, -2.4, and $+3.1$ kJ/mol, respectively. Hence, since more extensive benchmark studies indicate that the W1U method is more accurate than the CBS-QB3 method and since W1U reaction enthalpies for important reactions show smaller deviations with experimental data, simulations using the W1U values are expected to be more accurate. Indeed, as discussed later, simulations using W1U reaction enthalpies show a slight improvement in the predicted CH_4 yields. The CH_4 yield is found to be sensitive to the reaction enthalpy for C_2H_6 dissociation and the 2.9 kJ/mol higher W1U reaction enthalpy at 1000 K improves the predicted CH_4 yield.

The calculated heat capacities C_p at 298 K show a MAD of 0.8 J/(mol K) with available experimental data. Again, this value can be compared with deviations reported in the literature.[25] Reaction enthalpies calculated using the W1U method at 298 and at 1000 K are reported in Table 3 for the 150 elementary reactions in our kinetic model, and are compared with experimental data. The MAD for the W1U reaction enthalpies at 298 K, 2.4 kJ/mol, is better than the overall accuracy for the enthalpies of formation.

Ab initio rate coefficients for the 150 elementary reactions in our model are presented in an Arrhenius form in Table 3. Representative high pressure experimental rate coefficients at 1000 K were obtained from the NIST Chemical Kinetics Database[41] and are included for comparison. In general, the predicted ab initio rate coefficients are within a factor of four of the experimental values for all three families of reactions and the average deviation between experimental and calculated rate coefficients at 1000 K is a factor 1.7. For example, the calculated rate coefficient for the important C_2H_6 C-C scission reaction, 3.25×10^{-3} s^{-1}, is comparable

Table 4. Predicted and Industrial Yields of Major Products for Conditions I, II, and III in Table 1

	Ab Initio Predictions (wt %)											
	I-hp	I-hp	I-pdep	II-hp	II-hp	II-pdep	III-hp	III-hp	III-pdep	Industrial Data (wt %)		
	CBS-QB3	W1U	W1U	CBS-QB3	W1U	W1U	CBS-QB3	W1U	W1U	I	II	III
C_2H_6	39.3	39.7	40.1	40.0	40.5	41.0	47.4	47.7	48.3	39.3	39.0	48.9
C_2H_4	49.7	49.2	48.5	50.2	49.6	49.0	43.3	42.8	41.9	48.7	48.7	41.5
CH_4	2.9	3.3	3.5	2.0	2.3	2.5	2.5	2.8	3.0	3.4	3.0	2.2
H_2	3.6	3.5	3.5	3.8	3.7	3.7	3.1	3.0	2.9	3.7	3.7	3.1
C_3H_6	0.6	0.7	0.7	0.4	0.5	0.5	0.6	0.7	0.7	1.1	1.1	0.8
C_2H_2	0.7	0.7	0.6	0.8	0.7	0.6	0.4	0.4	0.3	0.2	–	–
Others	3.2	2.9	3.1	2.8	2.7	2.7	2.7	2.6	2.9	3.6	4.5	3.5
T_{out} (K)	1116	1111	1122	1116	1110	1121	1100	1095	1106	1133	1135	1110
P_{out} (atm)	1.9	1.9	1.9	1.6	1.6	1.6	2.4	2.4	2.4	1.9	1.6	2.4

I-hp, II-hp, and III-hp are modeled using high-pressure-limit rate coefficients. I-pdep, II-pdep, and III-pdep are modeled using pressure-dependent rate coefficients. CBS-QB3 (W1U) data were simulated using CBS-QB3 (W1U) enthalpies of formation.

with a recent experimental value, 4.5×10^{-3} s^{-1}. Finally, to illustrate the stringent accuracy demands required to predict conversions and yields, it should be noted that a 3.0 kJ/mol deviation in the activation energy or reaction enthalpy leads to a 50% change in the corresponding rate or equilibrium coefficient at 1000 K.

Ab initio simulations of an ethane steam cracker

Simulations Using High-Pressure-Limit Rate Coefficients. Steam cracking of ethane was first simulated for an industrial ethane cracker with a conversion of 59.9% (operating condition I in Table 1). For the first set of simulations we used the high-pressure-limit rate coefficients (I-hp), with CBS-QB3 enthalpies of formation or with W1U enthalpies of formation. The simulated yields for the major products C_2H_6, C_2H_4, CH_4, H_2, C_3H_6, and C_2H_2, as well as the simulated outlet temperature and pressure are compared with reported experimental values in Table 4. The mole fractions of C_2H_6, C_2H_4, CH_4, and H_2 along the reactor are shown in Figure 1a for operating condition I. At 1100 K, an equilibrium conversion of 66.2% is calculated for the $C_2H_6 \leftrightarrow C_2H_4 + H_2$ reaction using the W1U thermodynamic data. The predicted conversion at the reactor outlet, 60.3%, is similar to the industrial value of 59.9%. The mole fractions of the major radical species $\cdot C_2H_5$, $\cdot C_3H_5$, $\cdot CH_3$, $\cdot C_2H_3$, and $\cdot H$ are shown in Figure 1b. $\cdot C_2H_5$ is the dominant radical species, followed by the resonance stabilized $\cdot C_3H_5$ radical. The $\cdot CH_3$ concentration increases more rapidly in the second half of the reactor because the higher temperatures favor the dissociation of C_2H_6 to $\cdot CH_3$. The $\cdot C_2H_3$ radical also becomes more important in the second half of the reactor because of the higher temperatures and the higher C_2H_4 concentrations near the reactor outlet.

Even when using the computationally less demanding high-pressure-limit rate coefficients and the CBS-QB3 enthalpies, the predicted yields of C_2H_6, C_2H_4, and H_2 differ by less than 3% from the industrial data. The predicted CH_4 and C_3H_6 yields are somewhat low, while the C_2H_2 yield is severely over predicted. The total yield of other species (which mainly include molecules larger than C_3) is somewhat under predicted, likely because our reaction network does not include reactions forming larger species such as benzene. Using W1U instead of CBS-QB3 enthalpies of formation somewhat improves the predicted C_2H_4 yield, and brings the predicted CH_4 yield of 3.3 wt % close to the experimental value of 3.4 wt %. As discussed later, sensitivity analysis indicates that the predicted CH_4 yields are very sensitive to the values of several kinetic parameters in the model, with normalized yield change coefficients as large as 0.5, while the C_2H_6, C_2H_4 and H_2 yields are less sensitive with coefficients well below 0.1. The sensitivity analysis

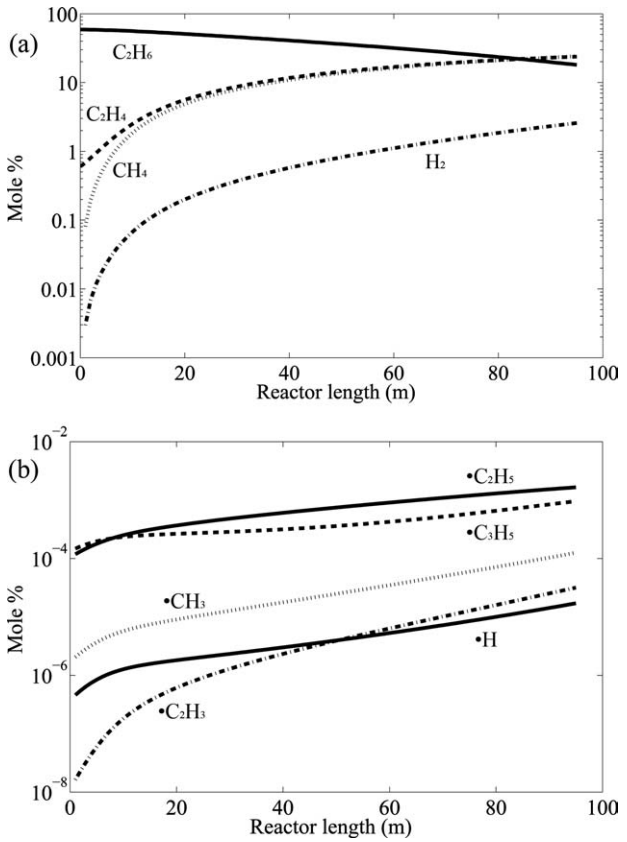

Figure 1. Mole fraction profiles along the reactor for the C_2H_6, C_2H_4, CH_4, and H_2 molecules (a) and for the $\cdot C_2H_5$, $\cdot C_3H_5$, $\cdot CH_3$, $\cdot C_2H_3$, and $\cdot H$ radicals (b) for the I-hp (W1U) simulations in Table 4.

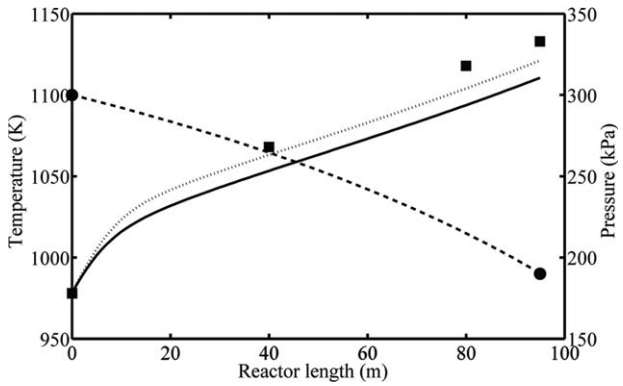

Figure 2. Reactor temperature and pressure profiles for operating condition I.

Temperature profile for the I-hp (W1U) simulations: solid line, for the I-pdep (W1U) simulations: dotted line; Pressure profile for the I-hp (W1U) simulations: dashed line; Experimental pressures: circles; Experimental temperatures: squares.

further shows that, to a large extent, the improved CH_4 yield can be attributed to the increased C_2H_6 dissociation rate coefficient when using the W1U enthalpies. A further increase in the CH_4 yield may be achieved by using a two-dimensional PFR model as suggested by Van Geem et al,[6] or, as shown later, by including the effect of pressure on the reaction rates. The predicted C_2H_2 yield is too high in all our simulations. This might be partially due to the neglect of coke formation. C_2H_2 is an important coke precursor and is incorporated seven times faster into coke than C_2H_4.[60] Coke formation might hence consume some of the C_2H_2. However, the typical coke yield is less than 0.1 wt % during ethane steam cracking[61] and coke formation alone cannot account for the high predicted C_2H_2 yields. Most of the C_2H_2 is formed via β-scission of $\cdot C_2H_3$ radicals, as also reported by Matheu and Grenda.[7] A detailed flux balance analysis[7] demonstrates that $\cdot C_2H_3$ radicals also add to olefins, ultimately leading to larger species such as benzene. Under high conversion ethane pyrolysis conditions and using a large reaction network, Matheu and Grenda find that only 25% of the $\cdot C_2H_3$ radicals lead to C_2H_2, while the majority adds to olefins, leading to products larger than C_3. Indeed, because of the low barrier, rate coefficients for $\cdot C_2H_3$ addition to olefins are significantly higher than the corresponding rate coefficients for $\cdot CH_3$ or $\cdot C_2H_5$ radicals, while the β-scission rate coefficient for $\cdot C_2H_3$ is similar to the value for $\cdot C_2H_5$ (Table 3). Unfortunately, our reaction network of 150 elementary reactions does not include many of the reactions involving molecules larger than C_3, and hence most of the $\cdot C_2H_3$ radicals are converted to C_2H_2 in our simulations. The high C_2H_2 yield therefore seems consistent with the low yield of larger molecules (''Others'' in Table 4) predicted by our ab initio kinetic model.

The reactor temperature and pressure profiles for the first set of simulations are shown in Figure 2. The simulated outlet temperature is 20 K lower than the temperature reported for the industrial reactor. A similar deviation is found for the other process conditions tested. A possible reason for the low predicted temperature is the use of a one-dimensional PFR model. Two-dimensional reactor simulations for a similar reactor geometry show radial temperature gradients of up to 50 K.[6] In addition, one should note that the simulated outlet temperature is very sensitive to the predicted yields. For the first operating condition, about 80% of the reactor heat input is consumed by the overall reaction enthalpy, while about 20% goes to $C_p\Delta T$ heat. The difference between the industrial and the predicted yields increases the overall reaction enthalpy by about 2%. This then leads to a 10% change in the temperature rise along the reactor, since the reactor heat input consumed by $C_p\Delta T$ decreases from 20% to 18% of the overall heat input. The pressure drop is described accurately by the one-dimensional reactor model.

The accuracy of the ab initio kinetic model was next tested for two additional operating conditions, one corresponding to a pilot-scale reactor with a tubular diameter of 1 cm and a residence time of 0.64 s, and another corresponding to an industrial split coil reactor with a lower inlet temperature of 898 K, a longer residence time of 1.2 s, and a lower ethane conversion of 51.1%. Using the high-pressure-limit rate coefficients and the CBS-QB3 reaction enthalpies (II-hp (CBS-QB3) and III-hp (CBS-QB3) in Table 4) the predicted yields of C_2H_6, C_2H_4, and H_2 again agree well with the experimental data. The largest deviation, 4%, is found for the C_2H_4 yield for condition III. The W1U reaction enthalpies slightly improve the predicted C_2H_4 yields, while the effect on the predicted H_2 yields and C_2H_6 conversions is small, as also observed for condition I. Using W1U reaction energies again increases the predicted CH_4 yield. For condition II, this improves the agreement with experimental data, while for condition III this slightly reduces the agreement. Predicted C_3H_6 yields are quite accurate for condition III, but too low for condition II. Predicted C_2H_2 yields again seem high, but no experimental data were reported for these cases. The predicted yield for the other products is too low, in particular for condition II. The simulated outlet temperatures are again slightly low.

Summarizing, the accuracy of the ab initio kinetic model seems to be consistent for the three cases. Predicted yields for C_2H_6, C_2H_4, and H_2 are within 5% of experimental data using only ab initio thermodynamic and kinetic parameters. Predicted CH_4 yields tend to be slightly low, but generally improve when more accurate W1U reaction energies are used. Except for the split coil reactor (case III), they improve further when pressure-dependent rate coefficients are used. Improving the predicted yields of C_2H_2, C_3H_6 and of molecules larger than C_3 likely requires an expansion of our reaction network.

Simulations Using Pressure-Dependent Rate Coefficients. High-conversion ethane pyrolysis simulations have indicated that some of the reactions are in the fall-off regime, affecting the yields of some of the minor products.[8] To evaluate the effect of the total pressure on the rate coefficients for $R_1 + R_2 \rightarrow P$, $R \rightarrow P_1 + P_2$, and $R \rightarrow P$-type reactions in our model, pressure-dependent rate coefficients were calculated at 1000 K, 2.5 atm and with steam as the bath gas using the QRRK-MSC method. Though more detailed Master Equation calculations[53] or simulations involving the complete pressure-dependent reaction network[62] would be needed to accurately predict yields under fall-off conditions, QRRK-MSC calculations have been found to be a reliable indicator of the effect of total pressure on the overall yields.[57]

Table 5. $k(T,P)/k_\infty(T)$ Ratios for Pressure-Dependent Reactions in the Ab Initio Kinetic Model at 1000 K, 2.5 atm and Using H_2O as the Bath Gas

	Reaction	$k(T,P)/k_\infty(T)$
1	$\cdot CH_3 + \cdot CH_3 \rightarrow C_2H_6$	0.90
2	$C_2H_6 \rightarrow \cdot CH_3 + \cdot CH_3$	0.73
3	$\cdot C_2H_5 + \cdot C_2H_5 \rightarrow C_4H_{10}$	1.00
4	$C_4H_{10} \rightarrow \cdot C_2H_5 + \cdot C_2H_5$	0.83
5	$\cdot CH_3 + \cdot C_2H_5 \rightarrow C_3H_8$	0.99
6	$C_3H_8 \rightarrow \cdot CH_3 + \cdot C_2H_5$	0.89
7	$\cdot C_2H_5 + \cdot H \rightarrow C_2H_6$	0.96
8	$C_2H_6 \rightarrow \cdot C_2H_5 + \cdot H$	0.42
9	$\cdot H + \cdot C_2H_3 \rightarrow C_2H_4$	0.85
10	$C_2H_4 \rightarrow \cdot H + \cdot C_2H_3$	0.75
11	$\cdot C_3H_5 + \cdot H \rightarrow C_3H_6$	0.93
12	$C_3H_6 \rightarrow \cdot C_3H_5 + \cdot H$	0.83
13	$\cdot H + \cdot C_3H_7 \rightarrow C_3H_8$	1.00
14	$C_3H_8 \rightarrow \cdot H + \cdot C_3H_7$	0.80
15	$\cdot CH_3 + \cdot C_2H_3 \rightarrow C_3H_6$	0.99
16	$C_3H_6 \rightarrow \cdot CH_3 + \cdot C_2H_3$	0.84
18	$H_2 \rightarrow \cdot H + \cdot H$	0.28
19	$\cdot C_2H_3 + \cdot C_2H_3 \rightarrow C_4H_6$	0.99
20	$C_4H_6 \rightarrow \cdot C_2H_3 + \cdot C_2H_3$	1.00
21	$\cdot C_2H_3 + \cdot C_2H_5 \rightarrow C_4H_8$	0.77
22	$C_4H_8 \rightarrow \cdot C_2H_3 + \cdot C_2H_5$	0.72
23	$\cdot CH_3 + \cdot H \rightarrow CH_4$	0.40
24	$CH_4 \rightarrow \cdot CH_3 + \cdot H$	0.34
25	$\cdot H + \cdot C_4H_9 \rightarrow C_4H_{10}$	1.00
26	$C_4H_{10} \rightarrow \cdot H + \cdot C_4H_9$	0.79
27	$\cdot H + \cdot 2\text{-}C_4H_9 \rightarrow C_4H_{10}$	1.00
28	$C_4H_{10} \rightarrow \cdot H + \cdot 2\text{-}C_4H_9$	0.80
29	$\cdot H + \cdot 2\text{-}C_3H_7 \rightarrow C_3H_8$	1.00
30	$C_3H_8 \rightarrow \cdot H + \cdot 2\text{-}C_3H_7$	0.83
31	$\cdot H + \cdot C_4H_7 \rightarrow C_4H_8$	1.00
32	$C_4H_8 \rightarrow \cdot H + \cdot C_4H_7$	0.61
33	$\cdot CH_3 + \cdot C_3H_7 \rightarrow C_4H_{10}$	1.00
34	$C_4H_{10} \rightarrow \cdot CH_3 + \cdot C_3H_7$	0.83
35	$\cdot CH_3 + \cdot C_3H_5 \rightarrow C_4H_8$	0.99
36	$C_4H_8 \rightarrow \cdot CH_3 + \cdot C_3H_5$	0.93
123	$C_2H_4 + \cdot H \rightarrow \cdot C_2H_5$	0.80
124	$\cdot C_2H_5 \rightarrow C_2H_4 + \cdot H$	0.62
125	$\cdot C_2H_5 + C_2H_4 \rightarrow \cdot C_4H_9$	0.97
126	$\cdot C_4H_9 \rightarrow \cdot C_2H_5 + C_2H_4$	0.80
127	$\cdot CH_3 + C_2H_4 \rightarrow \cdot C_3H_7$	0.87
128	$\cdot C_3H_7 \rightarrow \cdot CH_3 + C_2H_4$	0.85
129	$\cdot C_2H_3 + C_2H_4 \rightarrow \cdot C_4H_7$	0.94
130	$\cdot C_4H_7 \rightarrow \cdot C_2H_3 + C_2H_4$	0.75
131	$C_2H_2 + \cdot H \rightarrow \cdot C_2H_3$	0.28
132	$\cdot C_2H_3 \rightarrow C_2H_2 + \cdot H$	0.19
133	$\cdot CH_3 + C_2H_2 \rightarrow \cdot C_3H_5$	0.94
134	$\cdot C_3H_5 \rightarrow C_2H_2 + \cdot CH_3$	0.84
135	$C_3H_6 + \cdot H \rightarrow \cdot C_3H_7$	0.97
136	$\cdot C_3H_7 \rightarrow C_3H_6 + \cdot H$	0.74
137	$C_4H_6 + \cdot H \rightarrow \cdot C_4H_7$	0.98
138	$\cdot C_4H_7 \rightarrow C_4H_6 + \cdot H$	0.76
139	$C_4H_8 + \cdot H \rightarrow \cdot C_4H_9$	0.99
140	$\cdot C_4H_9 \rightarrow C_4H_8 + \cdot H$	0.74
141	$C_3H_6 + \cdot H \rightarrow \cdot 2\text{-}C_3H_7$	0.94
142	$\cdot 2\text{-}C_3H_7 \rightarrow C_3H_6 + \cdot H$	0.81
143	$C_4H_8 + \cdot H \rightarrow \cdot 2\text{-}C_4H_9$	0.52
144	$\cdot 2\text{-}C_4H_9 \rightarrow C_4H_8 + \cdot H$	0.52
145	$\cdot CH_3 + C_3H_6 \rightarrow \cdot 2\text{-}C_4H_9$	0.76
146	$\cdot 2\text{-}C_4H_9 \rightarrow C_3H_6 + \cdot CH_3$	0.73
147	$\cdot C_3H_7 \rightarrow \cdot 2\text{-}C_3H_7$	0.75
148	$\cdot 2\text{-}C_3H_7 \rightarrow \cdot C_3H_7$	0.80
149	$\cdot C_4H_9 \rightarrow \cdot 2\text{-}C_4H_9$	0.75
150	$\cdot 2\text{-}C_4H_9 \rightarrow \cdot C_4H_9$	0.50

High-pressure-limit rate coefficients for the reverse reactions were calculated using the W1U enthalpies of formation.

The ratios of the pressure-dependent rate coefficients $k(T,P)$ to the high-pressure-limit rate coefficients $k_\infty(T)$ are summarized for the affected reactions in Table 5. W1U enthalpies of reaction were used to calculate the high-pressure-limit rate coefficients. As shown in Table 5, most of the reactions show a modest effect of the total pressure under the conditions used in the simulations, though the effect is typically less than a factor two. For reactions of the type $A + B \leftrightarrow AB^* \rightarrow AB$, the dissociation rate of $AB^* \rightarrow A + B$ increases with temperature. At high temperatures, the dissociation rate of AB^* begins to compete with the stabilization of AB^* to AB through collisions and the overall rate $A + B \rightarrow AB$ reduces. The overall rate of $AB \leftrightarrow AB^* \rightarrow A + B$ type reactions also reduces at low bath gas pressures, as illustrated by a typical Lindemann mechanism.[53] Though the reduction of the rate coefficients due to fall-off is generally less than 50%, the rate coefficients for the reactions $H_2 \rightarrow \cdot H + \cdot H$, $\cdot CH_3 + \cdot H \rightarrow CH_4$, $CH_4 \rightarrow \cdot CH_3 + \cdot H$, $C_2H_2 + \cdot H \rightarrow \cdot C_2H_3$, and $\cdot C_2H_3 \rightarrow C_2H_2 + \cdot H$ are reduced to less than 40% of their high-pressure-limit rate coefficients. The fall-off behavior of these reactions can be expected to affect the yields of C_2H_2 and CH_4.

The steam cracking of ethane was next modeled for the three operating conditions using pressure-dependent rate coefficients (Table 4, I-pdep, II-pdep, III-pdep). Pressure-dependent rate coefficients change the yields of C_2H_6, C_2H_4 and H_2 by less than 2% for all three conditions. This is consistent with the simulations by Matheu and Grenda.[8] The use of pressure-dependent rate coefficients however increases the predicted CH_4 yields by about 10% and decreases the C_2H_2 yields by 15 to 25% for the three cases. As discussed, the change in yields also affects the predicted temperature rise along the reactor. For all three cases, slightly less heat is used for the overall reaction, and a somewhat larger temperature rise is simulated. This further improves the predicted outlet temperatures. The limited effect of pressure-dependent rate coefficients on the yields of C_2H_6, C_2H_4, and H_2 seems to be related to the limited sensitivity of those yields to the kinetic parameters. The yields for those three products are likely dominated by their thermodynamic properties, and fall-off effects have a limited influence on the ratio between the forward and reverse rate coefficients (Table 4). Yields of CH_4 and C_2H_2 are sensitive to the rate coefficients of several of the reactions that are predicted to be in the fall-off regime and are hence expected to change.

Sensitivity Analysis. To identify the kinetic parameters which have the largest effect on the predicted yields, a sensitivity analysis was conducted for the yields of C_2H_6, C_2H_4, H_2, CH_4, C_2H_2 and C_3H_6 and for the simulations using high-pressure-limit rate coefficients and W1U reaction enthalpies (case I-hp (W1U) in Table 4). To identify important reactions, the normalized yield change coefficients (Eq. 3) were calculated by increasing both the forward and reverse rate coefficients for each reaction pair by 10%. Note that this approach does not change the equilibrium coefficient for the reaction pair and hence maintains thermodynamic consistency.

Normalized yield change coefficients are shown in Figure 3 for the six major products. From Figure 3, it is clear that the normalized yield change coefficients for C_2H_6, C_2H_4, and H_2 are smaller than the coefficients for CH_4, C_2H_2, and C_3H_6. The predicted C_2H_6, C_2H_4, and H_2 yields are hence less

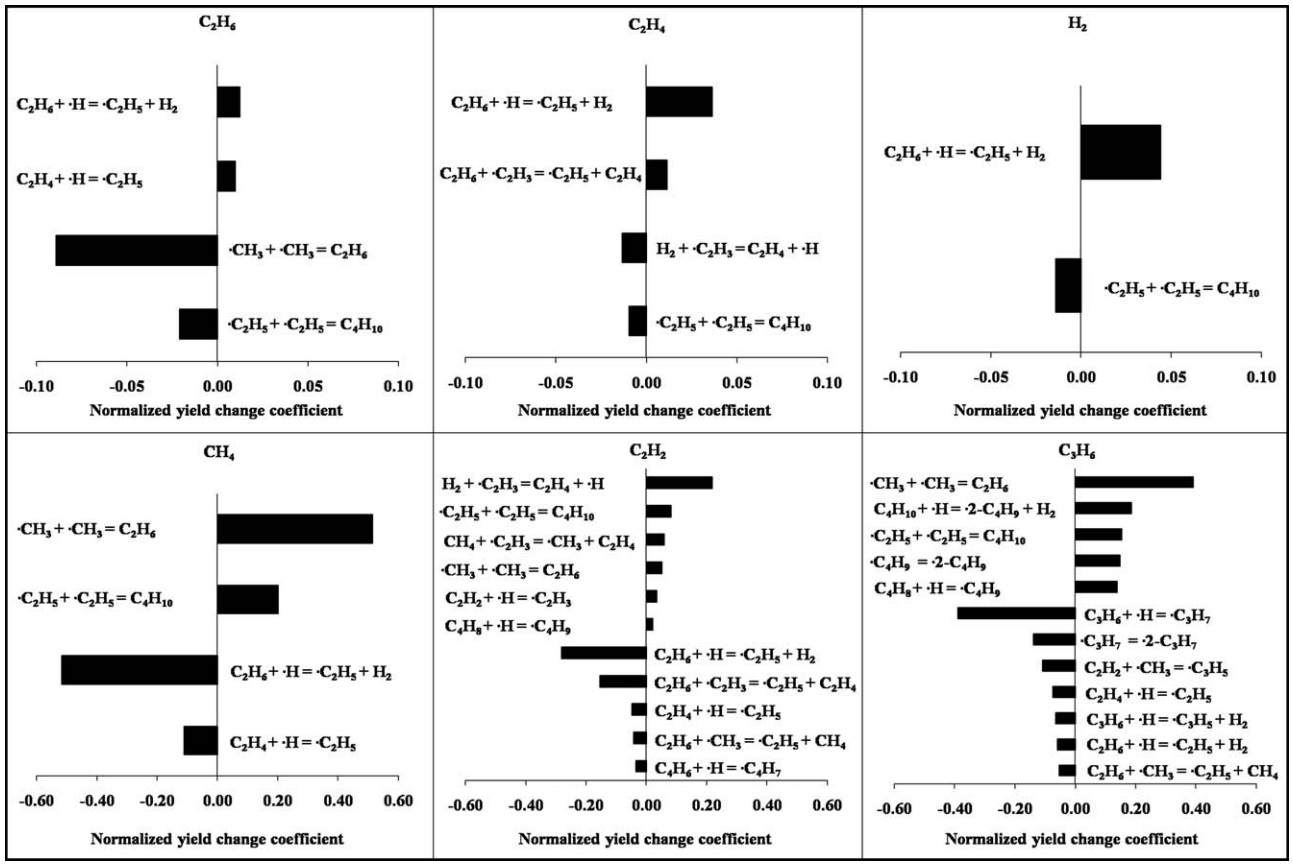

Figure 3. Normalized yield change coefficients (Eq. 3) for the major products C_2H_6, C_2H_4, H_2, CH_4, C_2H_2 and C_3H_6 for the I-hp (W1U) set of simulations in Table 4.

Only reactions with a yield change coefficient larger than 0.01 for C_2H_6, C_2H_4, and H_2, larger than 0.02 for C_2H_2, and larger than 0.05 for CH_4 and C_3H_6 are included.

sensitive to the values of the rate coefficients and are mainly determined by the thermodynamic parameters in the kinetic model. Indeed, increasing the rate coefficients for any of the reaction pairs in the model by a factor two changes the predicted yields for those three products by less than 10%. The C_2H_6 yield shows a modest sensitivity to the rate coefficients of the $C_2H_6 = \cdot CH_3 + \cdot CH_3$ initiation reaction and to the rate coefficients of the $\cdot C_2H_5 + \cdot C_2H_5 = C_4H_{10}$ reaction. Increasing both the forward and reverse rate coefficient of the $C_2H_6 = \cdot CH_3 + \cdot CH_3$ reaction increases the concentration of $\cdot CH_3$ radicals along the reactor. This increases the C_2H_6 conversion, and also the yields of C_2H_4, CH_4, C_3H_6, and C_2H_2. The yield of C_2H_4 is most sensitive to the rates of the hydrogen abstraction reactions, $C_2H_6 + \cdot H = \cdot C_2H_5 + H_2$ and also to the rates of the $\cdot C_2H_5 + \cdot C_2H_5 = C_4H_{10}$ reactions, which are a net consumer of $\cdot C_2H_5$ radicals.

The CH_4, C_2H_2, and C_3H_6 yields are much more sensitive to the calculated transition state properties, with normalized yield change coefficients of 0.52, −0.28, and −0.40, respectively. A 10% increase in the rates of the $C_2H_6 = \cdot CH_3 + \cdot CH_3$ reactions is calculated to change the CH_4 yield by 5.2%, while a 10% increase in the rates of the $C_2H_6 + \cdot H = \cdot C_2H_5 + H_2$ reactions decreases the CH_4 yield by 5.1%. Indeed, the yield of CH_4 will decrease while the H_2 yield will increase if more C_2H_6 is consumed by hydrogen abstraction by $\cdot H$ radicals. The kinetics of the $C_2H_4 + \cdot H = \cdot C_2H_5$ reactions are also important for the CH_4 yield, as also reported before.[4] C_3H_6 is mainly formed via the β-scission of $\cdot C_3H_7$ radicals and the C_3H_6 yield is sensitive to the kinetics of these reactions. Again, this reaction was identified by Matheu and Grenda[7] and by Van Geem et al.[6] The normalized yield change coefficient of −0.40 indicates that a 2.0 kJ/mol increase in the enthalpy of formation of the transition state for this reaction will increase the C_3H_6 yield by 11%. Finally, the sensitivity analysis identifies reactions involving $\cdot C_2H_3$ radicals, i.e., $C_2H_4 + \cdot H = H_2 + \cdot C_2H_3$ and $\cdot C_2H_3 = C_2H_2 + \cdot H$, as kinetically important to predict accurate C_2H_2 yields. Again, this finding is consistent with literature reports.[7]

Conclusions

An ab initio kinetic model consisting of 150 reversible elementary reactions and involving 20 species was constructed to simulate steam cracking of ethane. The thermodynamic and kinetic parameters in the model were obtained from CBS-QB3 and W1U quantum chemical calculations in combination with transition state theory. The importance of pressure-dependent rate coefficients was evaluated using the QRRK-MSC approach, but was found to be relatively minor under typical industrial ethane steam cracking conditions. The accuracy of the ab initio kinetic model was tested for three operating conditions reported

in the literature; an industrial reactor with a conversion of 60% and a residence time of 0.93 s, a pilot-scale reactor with a similar conversion, and an industrial split coil reactor with a conversion of 51% and a residence time of 1.2 s. C_2H_6 conversions, C_2H_4 and H_2 yields were predicted with an accuracy of better than 5% for the cases tested. The predicted yields of CH_4, C_2H_2 and C_3H_6 were found to be particularly sensitive to the accuracy of the kinetic parameters. Despite this high sensitivity, the predicted methane yields of 3.3, 2.3 and 2.8 wt % are comparable with experimental yields of 3.4, 3.0 and 2.2 wt %, respectively. Predicted C_2H_2 yields are somewhat high, which could be attributed to the limited size of the reaction network. Finally, to put the accuracy of the predicted yields and conversions into perspective, it should be noted that the MAD of 1.9 kJ/mol between the CBS-QB3 and the experimental enthalpies of formation translates to a 26% uncertainty in the predicted equilibrium coefficients at 1000 K.

This work hence illustrates that standard state-of-the-art quantum chemical calculations have become sufficiently accurate to begin to predict conversions and selectivities for large scale industrial processes such as ethane steam cracking. An extension to other complex radical reactions such as combustion, radical polymerization, and atmospheric chemistry can be envisioned. Ethane steam cracking was selected to limit the size of the reaction network, but the construction of a predictive ab initio kinetic model for naphtha and vacuum gasoil feedstock is in principle possible. For such large reaction networks, automated network generation[15,18,27] becomes indispensable, and group contribution methods,[22,24,26] group additivity methods[19–21,23,25] or structure-activity relationships[12,27] will be required to keep the number ab initio calculations tractable. Fortunately, the parameters for these methods can and have been derived from a limited set of accurate ab initio calculations.[21–25]

Acknowledgments

Financial support from the National University of Singapore is gratefully acknowledged.

Notation

C_p = heat capacity, J/(mol K)
c_0 = concentration in the standard state to which the translational partition function is referred, mol/m^3
ΔE_0(0 K) = energy difference between the transition state and the reactants at 0 K, including zero-point-energy, kJ/mol
h = Planck constant
$\Delta_f H$ = standard enthalpy of formation, kJ/mol
$k(T)$ = rate coefficient, m^3/(mol s)
k_B = Boltzmann constant
$k_{CVT}(T)$ = canonical variational transition state theory rate coefficient, m^3/(mol·s)
$k_\infty(T)$ = high-pressure-limit rate coefficient, m^3/(mol s) or 1/s
P = pressure, atm
$Q_i(T)$ = partition function of species i
R = gas constant, J/(K·mol)
s = reaction coordinate, pm
T = temperature, K
W_i = yield of species i

Greek letters

$\kappa(T)$ = tunneling correction factor
λ_{ij} = normalized yield change coefficient for species i and reaction j

Subscripts and superscripts

R = reactant
TS = transition state
out = reactor outlet

Literature Cited

1. Chauvel A, Lefebvre G. *Petrochemical Processes: Technical and Economic Characteristics*. Houston, TX: Gulf Publishing Company, 1989.
2. Van Damme PS, Narayanan S, Froment GF. Thermal cracking of propane and propane-propylene mixtures: pilot plant versus industrial data. *AIChE J*. 1975;21:1065–1073.
3. Froment GF, Van de Steene BO, Van Damme PS, Narayanan S, Goossens AG. Thermal cracking of ethane and ethane-propane mixtures. *Ind. Eng. Chem. Process Des. Dev*. 1976;15:495–504.
4. Sundaram KM, Froment GF. Modeling of thermal cracking kinetics. 3. Radical mechanisms for the pyrolysis of simple paraffins, olefins, and their mixtures. *Ind. Eng. Chem. Fundam*. 1978;17:174–182.
5. Belohlav Z, Zamostny P, Herink T. The kinetic model of thermal cracking for olefins production. *Chem. Eng. Process*. 2003;42:461–473.
6. Van Geem KM, Heynderickx GJ, Marin GB. Effect of radial temperature profiles on yields in steam cracking. *AIChE J*. 2004;50:173–183.
7. Matheu DM, Grenda JM. A systematically generated, pressure-dependent mechanism for high-conversion ethane pyrolysis. 1. Pathways to the minor products. *J. Phys. Chem. A* 2005;109:5332–5342.
8. Matheu DM, Grenda JM. A systematically generated, pressure-dependent mechanism for high-conversion ethane pyrolysis. 2. Radical disproportionations, missing reaction families, and the consequences of pressure dependence. *J. Phys. Chem. A* 2005;109:5343–5351.
9. Van Goethem MWM, Barendregt S, Grievink J, Moulijn JA, Verheijen PJT. Towards synthesis of an optimal thermal cracking reactor. *Chem. Eng. Res. Des*. 2008;86:703–712.
10. Sadrameli SM, Green AES. Systematics and modeling representations of naphtha thermal cracking for olefin production. *J. Anal. Appl. Pyrolysis* 2005;73:305–313.
11. Kumar P, Kunzru D. Modeling of naphtha pyrolysis. *Ind. Eng. Chem. Process Des. Dev*. 1985;24:774–782.
12. Broadbelt LJ, Stark SM, Klein MT. Computer generated pyrolysis modeling: on-the-fly generation of species, reactions, and rates. *Ind. Eng. Chem. Res*. 1994;33:790–799.
13. De Witt MJ, Dooling DJ, Broadbelt LJ. Computer generation of reaction mechanisms using quantitative rate information: application to long-chain hydrocarbon pyrolysis. *Ind. Eng. Chem. Res*. 2000;39:2228–2237.
14. Ranzi E, Dente M, Pierucci S, Blardl G. Initial product distributions from pyrolysis of normal and branched paraffins. *Ind. Eng. Chem. Fundam*. 1983;22:132–139.
15. Van Geem KM, Reyniers MF, Marin GB, Song J, Green WH, Matheu DM. Automatic reaction network generation using RMG for steam cracking of n-hexane. *AIChE J*. 2006;52:718–730.
16. Dente MD, Bozzano G, Faravelli T, Marongiu A, Pierucci S, Ranzi E. Kinetic modelling of pyrolysis processes in gas and condensed phase. In: Marin GB, editor. *Advances in Chemical Engineering*, Volume 32. New York: Academic Press; 2007:51–166.
17. Pant KK, Kunzru D. Pyrolysis of methylcyclohexane: kinetics and modeling. *Chem. Eng. J*. 1997;67:123–129.
18. Clymans PJ, Froment GF. Computer-generation of reaction paths and rate equations in the thermal cracking of normal and branched paraffins. *Comput. Chem. Eng*. 1984;8:137–142.
19. Benson SW. *Thermochemical Kinetics, 2nd ed*. New York: Wiley, 1976.
20. Cohen N. Thermochemistry of alkyl free radicals. *J. Phys. Chem*. 1992;96:9052–9058.
21. Sumathi R, Carstensen HH, Green WH Jr. Reaction rate prediction via group additivity part 1: H abstraction from alkanes by H and CH_3. *J. Phys. Chem. A* 2001;105:6910–6925.s
22. Saeys M, Reyniers, MF, Marin, GB, Van Speybroeck V, Waroquier M. *Ab initio* group contribution method for activation energies for radical additions. *AIChE J*. 2004;50:426–444.
23. Sabbe MK, Saeys M, Reyniers MF, Marin GB, Van Speybroeck V, Waroquier M. Group additive values for the gas phase standard enthalpy of formation of hydrocarbons and hydrocarbon radicals. *J. Phys. Chem. A* 2005;109:7466–7480.

24. Saeys M, Reyniers MF, Van Speybroeck V, Waroquier M, Marin GB. *Ab initio* group contribution method for activation energies of hydrogen abstraction reactions. *ChemPhysChem* 2006;7:188–199.
25. Sabbe MK, De Vleeschouwer F, Reyniers MF, Waroquier M, Marin GB. *Ab initio* based group additive values for the gas phase standard entropy and heat capacity of hydrocarbons and hydrocarbon radicals. *J. Phys. Chem. A* 2008;112:12235–12251.
26. Willems PA, Froment GF. Kinetic modeling of the thermal cracking of hydrocarbons. 1. Calculation of frequency factors. *Ind. Eng. Chem. Res.* 1988;27:1959–1971.
27. Broadbelt LJ, Pfaendtner J. Lexicography of kinetic modeling of complex reaction networks. *AIChE J.* 2005;51:2112–2121.
28. Martin JML, de Oliveira G. Towards standard methods for benchmark quality *ab initio* thermochemistry—W1 and W2 theory. *J. Chem. Phys.* 1999;111:1843–1856.
29. Montgomery JA Jr, Frisch MJ, Ochterski JW, Petersson GA. A complete basis set model chemistry. VI. Use of density functional geometries and frequencies. *J. Chem. Phys.* 1999;110:2822–2827.
30. Montgomery JA, Jr., Frisch MJ, Ochterski JW. Petersson GA. A complete basis set model chemistry. VII. Use of the minimum population localization method. *J. Chem. Phys.* 2000;112:6532–6542.
31. Saeys M, Reyniers MF, Marin GB, Van Speybroeck V, Waroquier M. *Ab initio* calculations for hydrocarbons: enthalpy of formation, transition state geometry, and activation energy for radical reactions. *J. Phys. Chem. A* 2003;107:9147–9159.
32. Vansteenkiste P, Van Speybroeck V, Marin GB, Waroquier M. *Ab initio* calculation of entropy and heat capacity of gas-phase n-alkanes using internal rotations. *J. Phys. Chem. A* 2003;107:3139–3145.
33. Sun W, Saeys M. *Ab initio* study of the reaction of formic and acetic acids with hydroxyl radicals. *J. Phys. Chem. A* 2008;112:6918–6928.
34. Kungwan N, Truong TN. Kinetics of the hydrogen abstraction $\cdot CH_3$ + Alkane $\rightarrow$ CH_4 + Alkyl reaction class: An application of the reaction class transition state theory. *J. Phys. Chem. A* 2005;109:7742–7750.
35. Vandeputte AG, Sabbe MK, Reyniers MF, Van Speybroeck V, Waroquier M, Marin GB. Theoretical study of the thermodynamics and kinetics of hydrogen abstractions from hydrocarbons. *J. Phys. Chem. A* 2007;111:11771–11786.
36. Sabbe MK, Vandeputte AG, Reyniers MF, Van Speybroeck V, Waroquier M, Marin GB. Ab initio thermodynamics and kinetics for carbon-centered radical addition and β-scission reactions. *J. Phys. Chem. A* 2007;111:8416–8428.
37. Harding LB, Georgievskii Y, Klippenstein SJ. Predictive theory for hydrogen atom-Hydrocarbon radical association kinetics. *J. Phys. Chem. A* 2005;109:4646–4656.
38. Klippenstein SJ, Georgievskii Y, Harding LB. Predictive theory for the combination kinetics of two alkyl radicals. *Phys. Chem. Chem. Phys.* 2006;8:1133–1147.
39. Wauters S. Kinetics of coke formations during thermal cracking of hydrocarbons based on elementary reactions, Ph.D. thesis, Ghent University, Ghent, Belgium, 2001.
40. Afeefy HY, Liebman JF, Stein SE. Neutral thermochemical data. In: Linstrom PJ, Mallard WG, editors. NIST Chemistry WebBook, NIST Standard Reference Database Number 69, June 2005, National Institute of Standards and Technology, Gaithersburg MD, 20899. Available at http://webbook.nist.gov.
41. NIST Chemical Kinetics Database: Standard Reference Database 17, Version 7.0 (Web Version), Release 1.4. Available at http://kinetics.nist.gov/kinetics/index.jsp.
42. Benson SW, Haugen GR. A simple, self-consistent electrostatic model for quantitative prediction of the activation energies of four-center reactions. *J. Am. Chem. Soc.* 1965;87:4036–4044.
43. Frisch MJ, Trucks GW, Schlegel HB, Scuseria GE, Robb MA, Cheeseman JR, Montgomery JA, Jr., Vreven T, Kudin KN, Burant JC, Millam JM, Iyengar SS, Tomasi J, Barone V, Mennucci B, Cossi M, Scalmani G, Rega N, Petersson GA, Nakatsuji H, Hada M, Ehara M, Toyota K, Fukuda R, Hasegawa J, Ishida M, Nakajima T, Honda Y, Kitao O, Nakai H, Klene M, Li X, Knox JE, Hratchian HP, Cross JB, Bakken V, Adamo C, Jaramillo J, Gomperts R, Stratmann RE, Yazyev O, Austin AJ, Cammi R, Pomelli C, Ochterski JW, Ayala PY, Morokuma K, Voth GA, Salvador P, Dannenberg JJ, Zakrzewski VG, Dapprich S, Daniels AD, Strain MC, Farkas O, Malick DK, Rabuck AD, Raghavachari K, Foresman JB, Ortiz JV, Cui Q, Baboul AG, Clifford S, Cioslowski J, Stefanov BB, Liu G, Liashenko A, Piskorz P, Komaromi I, Martin RL, Fox DJ, Keith T, Al-Laham MA, Peng CY, Nanayakkara A, Challacombe M, Gill PMW, Johnson B, Chen W, Wong MW, Gonzalez C, Pople JA. Gaussian 03, Revision C.02; Gaussian, Inc., Wallingford CT, 2004.
44. Mcquarrie DA. *Statistical Mechanics*. Sausalito, CA, U.K.: University Science Books, 2000.
45. Andersson MP, Uvdal P. New scale factor for harmonic vibrational frequencies using the B3LYP density functional method with the triple-ζ basis set 6–311+G(d,p). *J. Phys. Chem. A* 2005;109:2937–2941.
46. Pollak E, Pechukas P. Symmetry numbers, not statistical factors, should be used in absolute rate theory and in Brønsted relations. *J. Am. Chem. Soc.* 1978;100:2984–2991.
47. Eckart C. The penetration of a potential barrier by electrons. *Phys. Rev.* 1930;35:1303–1309.
48. Corchado JC, Chuang YY, Fast PL, Hu WP, Liu YP, Lynch GC, Nguyen KA, Jackels CF, Ramos AF, Ellingson BA, Lynch BJ, Melissas VS, Villà J, Rossi I, Coitiño EL, Pu J, Albu TV, Steckler R, Garrett BC, Isaacson AD, Truhlar DG. POLYRATE, version 9.7; University of Minnesota: Minneapolis, MN, 2007.
49. Corchado JC, Chuang YY, Coitiño EL, Truhlar DG. GAUSSRATE, version 9.7; University of Minnesota: Minneapolis, MN, 2007.
50. Isaacson AD, Truhlar DG. Polyatomic canonical variational theory for chemical reaction rates. Separable-mode formalism with application to OH + H_2→ H_2O + H. *J. Chem. Phys.* 1982;76:1380–1391.
51. Rosenman E, McKee ML. Reaction-path dynamics and theoretical rate constants for the CH_3F + Cl → HCl + CH_2F reaction by direct dynamics method. *J. Am. Chem. Soc.* 1997;119:9033–9038.
52. Villa J, Corchado JC, Gonzalez-Lafont A, Lluch JM, Truhlar DG. Variational transition-state theory with optimized orientation of the dividing surface and semiclassical tunneling calculations for deuterium and muonium kinetic isotope effects in the free radical association reaction H + C_2H_4 → C_2H_5. *J. Phys. Chem. A* 1999;103:5061–5074.
53. Wendell F. *Unimolecular Reactions: a Concise Introduction*. New York: Cambridge University Press, 2003.
54. Schwenke DW. A theoretical prediction of hydrogen molecule dissociation-recombination rates including an accurate treatment of internal state nonequilibrium effects. *J. Chem. Phys.* 1990;92:7267–7282.
55. Kassel LS. Studies in homogeneous gas reactions. II. Introduction of quantum theory. *J. Phys. Chem.* 1928;32:1065–1079.
56. Dean AM. Predictions of pressure and temperature effects upon radical addition and recombination reactions. *J. Phys. Chem.* 1985;89:4600–4608.
57. Chang AY, Bozzelli JW, Dean AM. Kinetic analysis of complex chemical activation and unimolecular dissociation reactions using QRRK theory and the modified strong collision approximation. *Z. Phys. Chem.* 2000;214:1533–1568.
58. Turanyi T. Applications of sensitivity analysis to combustion chemistry. *Reliab. Eng. Syst. Saf.* 1997;57:41–48.
59. Barnes EC, Petersson GA, Montgomery JA Jr, Fris MJ, Martin JML. Unrestricted coupled cluster and Brueckner doubles variations of W1 theory. *J. Chem. Theory. Comput.* 2009;5:2687–2693.
60. Kopinke FD, Zimmermann G, Nowak S. On the mechanism of coke formation in steam cracking—conclusions from results obtained by tracer experiments. *Carbon* 1988;26:117–124.
61. Velenyi LJ, Song Y, Fagley JC. Carbon deposition in ethane pyrolysis reactors. *Int. Eng. Chem. Res.* 1991;30:1708–1712.
62. Matheu DM, Green WH Jr, Grenda JM. Capturing pressure-dependence in automated mechanism generation: reactions through cycloalkyl intermediates. *Int. J. Chem. Kinet.* 2003;35:95–119.

Manuscript received Apr. 28, 2010, and revision received Sept. 15, 2010.